Developing a Model for CD8+ T-cell Recognition of Pancreatic Cancer and its Metastases

Anne Flier[1], Megan T. Hoffman[1,2], Victoria Lippert[1], Stephanie Dougan[1,2].

[1] Department of Cancer Immunology and Virology, Dana-Farber Cancer Institute, Boston, MA, USA.

[2] Department of Immunology, Harvard Medical School, Boston, MA, USA.

MSc Minor research project report, Infection & Immunity, Utrecht University

Research group: Stephanie Dougan, Cancer Immunology and Virology, Dana-Farber Cancer Institute, Department of Immunology, Harvard Medical School.

Daily supervisor: Megan Hoffman

Examiners: Stephanie Dougan and Marianne Boes

Start date: 16-01-2022

End date: 26-08-2022

Total ECTS (x+y): 39

Abstract

Outgrowth of undetectable micrometastasis in patients with localized pancreatic ductal adenocarcinoma (PDAC) results in a 5-year survival rate of only 42%. To understand the involvement of the immune system during the establishment and outgrowth of micrometastasis, we developed a novel mouse model in which metastases can be studied after complete resection of the primary pancreatic tumor. In this model, we found that T-cell depletion post tumor resection did not increase the number of grown out micrometastasis, indicating a lack of T-cell response, potentially due to an absence of good tumor antigens. To study metastasis in the context of a recognizable tumor antigen, we transfected pancreatic cancer cells with the physiologically relevant melanoma self-antigen tyrosinase related protein 1 (TRP1). We generated a metastatic cell line expressing TRP1 from established metastasis after subsequent intravenous and subcutaneous injections. In our mouse model, these metastatic TRP1 cells gave rise to high T-cell infiltrated tumors that poorly metastasize, which contrasts greatly with metastatic PDAC lines lacking TRP1 expression. We examined the metastasis that did occur for the presence of TRP1 expression, but we were unable to detect it, suggesting evidence for immunoediting. Altogether, our study highlights a role for T-cells in pancreatic metastasis in the presence of a recognizable tumor antigen.

Laymen's summary

Pancreatic ductal adenocarcinoma (PDAC) is a highly aggressive cancer that accounts for 90% of all pancreatic cancers. The 5-year survival rate is 11%, placing it among the most lethal of all cancers. The main contributor to this poor prognosis is the high prevalence of metastasis (seeding of cancer cells in distant organs) at the time of diagnosis. Moreover, less than half of the patients that present with only a localized tumor in the pancreas survive 5 years post diagnosis. This is linked to the ability of PDAC to metastasize early in disease progression, resulting in the presence of undetectable, small metastasis (micrometastasis). These micrometastasis grow out to macrometastasis and are an important factor for the high mortality rate in patients with localized disease. The immune system would be ideally suited to target and clear those metastasis but immunotherapies in PDAC have shown limited success. Therefore, it is essential to understand the role of immune cells during the establishment and outgrowth of pancreatic metastasis, especially T-cells, as they can specifically target and kill cancerous cells. To study metastasis our lab developed a new mouse model. In short, we inject pancreatic tumor cells subcutaneously into the back of a mouse, wait for a primary tumor to develop, then remove this tumor and after a few weeks we can find clear lung or lymph node metastasis. To investigate the role of T-cells specifically during the outgrowth of micrometastasis, we depleted T-cells, including tumor specific T-cells, after resection of the tumor. By doing so, we could test if T-cells are able to prevent outgrowth of micrometastasis. Strikingly, we found that T-cell depletion did not alter the number of metastasis, indicating an absence of T-cell control of micrometastasis. Data from other studies show that the absence of T-cell mediated immune control is due to the lack of tumor specific proteins (tumor antigens). Thus, we worked to generate a pancreatic cancer cell line that expresses the recognizable tumor antigen tyrosinase related protein 1 (TRP1). TRP1 is expressed in skin cancer tumors in both mice and humans and immunologically resembles tumor antigens, because like most tumor antigens, TRP1 does not induce a strong immune response. To use this cell line to study metastasis, we selected for metastatic cells in two subsequent rounds. We collected tumor cells from lung metastasis that have established after intravenous injection then, subcutaneously injected them in our resectable mouse model where, again, we isolated cells from a lung metastasis. Via this way we selected for cells that can both escape from the primary tumor and seed in distant organs. To eventually study T-cell associated immunity in the context of metastasis, we injected these metastatic TRP1 cells in our novel mouse model. We found that the T-cell presence in primary TRP1 tumors is much higher than in tumors without TRP1. Interestingly, when we assessed the metastatic burden of the metastatic TRP1 cells, we found few metastasis. We checked if the tumor cells in those metastasis still expressed TRP1, but could not detect any. Together, these results highlight a role for T-cells in the establishment of pancreatic cancer micrometastasis in the presence of the recognizable tumor antigen TRP1 and pave way for further studies into the involvement of the immune system during pancreatic cancer.

Introduction

In pancreatic ductal adenocarcinoma (PDAC) the majority of patients present with distant metastasis, while only 40% of patients are diagnosed with localized disease [1,2]. Standard of care therapy for non-metastatic tumors is surgical removal of the tumor alongside chemotherapy [3]. However, only 42% of patients with localized and resected PDAC survive until 5-years after diagnosis [4]. The main contributor to this poor prognosis is the high relapse rate after surgery. In two-thirds of cases tumors are found at distal sites [5], illustrating that even a small, localized tumor can lead to undetectable metastasis prior to surgery [6,7]. Therefore, it is especially important to understand the mechanism behind the establishment of micrometastatic disease even from localized PDAC tumors.

The most commonly used *in vivo* model that recapitulates the development and occurrence of PDAC in humans is the is LSL-*Kras*$^{G12D/+}$; LSL-*Trp53*$^{R172H/+}$; *Pdx1−Cre* (KPC) mouse model [8,9]. This model closely resembles the progression and growth of PDAC from a normal pancreas, including the presence of metastasis. However, because this is a stochastic model, the timing of metastasis is variable per animal, making it a difficult model to use for comprehensive studies [8]. A more common model of metastasis uses intravenous injection of tumor cells in the tail vein or the splenic vein [10–14]. This models generates robust lung or liver metastasis through the injection of a large bolus of cells. However, intravenous injection models only study the extravasation and establishment of tumor cells in the secondary site, leaving the role of the primary tumor and extravasation unexplored [15]. Therefore, we developed a novel mouse model that recapitulates the occurrence of micrometastasis from an intact primary tumor.

Our mouse model of resectable pancreatic cancer uses a mouse cancer cell line derived from KPC cells, specifically the KPC-6694C2 (C2) cells [16]. In this model we inject C2 cells subcutaneously in the back of C57BL/6J mice and allow tumors to establish for 11 days. Following complete resection of the primary tumor, mice are monitored for lung and lymph node metastasis between 4 to 5 weeks post-surgery. To ensure a consistently high metastatic phenotype, we generated a cell line from a C2 lung metastasis, giving rise to the KPC-C2-SQ-lungmet cell line (in short C2-met). The usage of these cells resulted in an over 40% increase in lung metastasis when compared to the parental C2 cell line. Thus, this model gives us the opportunity to study the role of immune cells during the establishment and outgrowth of pancreatic metastasis.

PDAC has been associated with T-cell paucity, exclusion and exhaustion, limiting the ability of immune targeting of the cancer cells [17,18]. As a consequence, immunotherapies in PDAC have shown very limited success [19]. This decreased T-cell function is mainly due to the presence of a desmoplastic immunosuppressive tumor microenvironment and the low mutational burden of PDAC tumors [20–

22]. In fact, it has been shown that T-cell depletion in KPC mice has no effect on overall mouse survival [23]. However, introduction of the strong neoantigen ovalbumin (OVA) in KPC cells, leads to curing of subcutaneously injected tumors in a T-cell dependent manner [23]. This highlights that the lack of T-cell response is, in part, due to an absence of recognizable tumor antigens. We wanted to expand on these results and investigate how expression of a more physiological relevant antigen affects primary tumor growth and metastasis.

Tyrosinase related protein 1 (TRP1) is an intermembrane enzyme that is involved in the production of melanin by melanocytes [24]. Melanoma tumors, such as B16, express high levels of TRP1 both in humans and mice while the natural immune response against these tumors is weak [25–27]. However, significant improvements in patient survival have been made by co-treating patients with chemotherapy and immunotherapy [28]. In cancers, including PDAC, many tumor antigens, like TRP1, are often mutated or overexpressed self-antigens which result in low affinity T-cell responses [21,22,29]. In mice, adoptive transfer of a TRP1 chimeric antigen receptor (CAR) T-cell cocktail drastically increased survival of B16 tumor bearing mice [30], illustrating that targeting tumor antigens could inhibit disease progression. To take advantage of TRP1 overexpression in melanoma, and beyond, our lab developed transnuclear mice generating TRP1 specific T-cells with which we can now probe the role of T-cell recognition in the context of an weak self-antigen in any cancer [31]. We generated and characterized a KPC-C2 TRP1 expressing cell line to provide a platform to study involvement of T-cell mediated tumor control in the presence of a low affinity antigen.

In our current study, we investigated the importance of T-cell associated immunity during PDAC metastasis. We found that T-cell depletion after tumor resection did not affect macrometastatic burden in C2-met tumor-bearing mice, suggesting a lack of T-cell control. We then generated a metastatic TRP1 expressing C2 cell line. During this work, we found a consistent decrease in metastasis from TRP1 expressing primary tumors corresponding with a high CD8+ T-cell infiltration. Interestingly, the metastasis which do arise from the metastatic TRP1 C2 cells have undetectable levels of TRP1 and decreased levels of the co-expressed marker zsGreen. This may indicate that immunoediting results in antigen loss at the metastatic sites. Altogether, our study highlights a role for T-cells in the establishment of pancreatic cancer micrometastasis in the presence of a recognizable tumor antigen, which paves way for further studies into the involvement of the immune system during pancreatic cancer.

Materials and Methods

Animal care

Animals were housed at the Dana-Farber Cancer Institute (DFCI) and were maintained according to protocols approved by the DFCI Institute Committee on Animal Care and Use. C57BL/6J mice were purchased from Jackson Labs. Age matched 8-10 week old female mice were used for each experiment.

Tumor cell line generation

The KPCY-6694C2 (KPCY-C2) cell line was derived from a LSL-*Kras*$^{G12D/+}$;LSL-*Trp*53$^{R172H/+}$;*Pdx1−Cre* (KPC), YFP-floxed mouse and was kindly provided by Ben Stanger's lab [16]. Generation of the C2-met was derived from a lung metastasis,

For the C2-VTRP1 cell line, a pEF1a-IRES-zsGreen plasmid was produced in *E. coli*. In this vector, the multiple cloning site is located downstream of the promotor pEF1, followed by internal ribosome entry site 2 (IRES2) and the zsGreen gene. Further downstream, resistance markers for kanamycin (KanR) and neomycin (NeoR) are located under a SV40 promotor. TRP1 was cloned into the MSC of this vector by restriction enzyme digest (EcoRI + BamHI) followed by ligation with T4 ligase. Bacteria were transfected and cultured on kanamycin plates to select for successful transfection. Plasmid was isolated with the E.Z.N.A.® Plasmid DNA Mini Kit I (OMEGA) and used to stable transfect KPCY-6694C2 cells. Cells were sorted, collecting a fraction of high zsGreen+ cells. Overexpression of TRP1 was validated in each cell line by western blot.

B16 cells were purchased from American Type Culture Collection. To generate fluorescently labelled B16, B16 cells were transfected with a zsGreen-overexpression plasmid. Here, zsGreen is located downstream of the pUbc promotor followed by a P2A sequence. Cells were selected by culturing with hygromycin for successful transfection, and overexpression was validated in each cell line by RT-qPCR for zsGreen.

Cells were only used in low passage for each experiment.

Tumor cell culture

Cells were cultured in sterile filtered RPMI-1640 media (Gibco, #11875-093) supplemented with 10% heat inactivated fetal bovine serum (FBS) (Gibco), 2 mmol/l L-glutamine (GlutaMax, Gibco), 1% v/v penicillin/streptomycin (PenStrep, Gibco), 1% v/v minimal essential media non-essential amino acids (MEM NEAA, Gibco) and 1 mmol/l sodium pyruvate (Gibco), from heron referred to as RPMI complete. TRP1 expressing cells were continuously cultured with 400 µg/ml geneticin (Gibco, 10131-035) to select for cells expressing the TRP1 plasmid. All cells were incubated at 37 ^{o}C, 5% CO_2 in a humidified incubator. When confluency reached between 50-100%, cells were washed with PBS (Gibco) and collected after 0.25% trypsin-EDTA (Gibco) treatment. Cells were counted using a hemocytometer

(Hausser Scientific), spun down at 390*g,* 5 minutes, 4 °C and diluted to desired concentration. Cells were no longer used after 12 passages. For long term storage, the lowest passages were resuspended in 10% v/v DMSO (Sigma) in heat inactivated FBS, allowed to slowly freeze at -80 °C for 48 hours and then stored at -140 °C in liquid nitrogen indefinitely.

Mouse model of resectable pancreatic cancer

Prior to tumor injection mice were sedated with 3% isoflurane. Mouse backs were shaved and subsequently (SQ) injected with 200,000 tumor cells in 150 µl Hank's Balanced Salt Solution (HBSS, Gibco) per mouse. Between each injection the syringe tip was wiped to remove excess cells. After injection, all mice were randomized. When tumors reached maximum size before ulceration (11 – 14 days post injection) all mice were simultaneously taken for surgery. Mice were anesthetized with a ketamine/xylazine cocktail injected intraperitoneally and treated with meloxicam in the neck subcutaneously. After tumor resection, wound was treated with ropivacaine and closed with metal wound clips. Mice were treated with meloxicam until 2 days post-surgery. Tumors were carefully weighed then taken for further analysis. Mice were sacrificed 4-5 weeks later, or earlier if humane endpoint was reached prematurely, by 50% CO_2 for 5 minutes, followed by cervical dislocation. Mouse lungs and lymph nodes were collected to count macroscopic metastatic lesions. Mice that regrew tumors were excluded from analysis.

To study the influence of tumor specific T-cells, mice were intraperitoneally injected with a mixture of CD4 (InVivoMab, BE003.1) or CD8 (InVivoMab, BE006.1) antibodies at a concentration of 100 µg per mouse in 100 µl endotoxin free PBS (TMS-012-A Endotoxin-Free Dulbecco's PBS, EMD Milipore Comp.) or isotype control rat IgG2 (InVivoMab, BE009.0). Injections were given directly after surgery and two-days post-surgery.

Four hours prior to adoptive transfer of $TRP1^{high}$ cells, mice were lightly irradiated with 100 rads. $TRP1^{high}$ immune cells were taken from a 4-6 weeks old C57BL6/J female mouse. Spleen, mesenteric, inguinal, brachial, superficial cervical lymph nodes were harvested and homogenized through a 40 µm filter using a sterile syringe plunger into PBS. Cells were spun down at 390*g,* 4 minutes, 4 °C, thoroughly resuspended in 1 ml ACK lysis buffer (8.26 g/ml ammonium chloride (Sigma, #A9434), 1 g/l potassium bicarbonate (Sigma, #237205), 37 mg/l EDTA (Sigma, #E5134) in deionized water) for 30 seconds and neutralized by adding 3 ml PBS. Cells were spun down and resuspended in HBSS. Mice were warmed on heating pad and intravenously injected into the tail vein with 150 µl immune cells representing 4.7 million cells per mouse. Cells were allowed to establish for 1 day.

To derive a metastatic C2-VTRP1 cell line, we first utilized the intravenous (IV) tumor cell injection metastasis model [10–14]. Mice were warmed on heating pad and then intravenously injected with

50,000 C2-VTRP1 WT cells in 150 µl HBSS through the tail vein. Mice were sacrificed two weeks post-injection. Lungs were collected and several macroscopic lesions were isolated.

Flow cytometry on immune cells from murine samples

Immune cells were analyzed from larger subcutaneous tumors to ensure high cell number following digestion. Tumors were minced and incubated in 0.5 µg/ml soybean trypsin inhibitor (Gibco, 17075029), 50 µg/ml collagenase IV (Sigma, C5138) in RPMI-1640 media for 30 minutes, 37 °C. Remaining tumor chunks were manually degraded by repeatedly pipetting up and down, after which cell suspension was filtered through a 40 µm filter into FACS tubes to retrieve single cells. Cells were washed twice with FACS buffer (2% FBS, 1 mM UltraPure™ 0.5M EDTA (Life Technologies, 15575020) in PBS) and spun at 390*g*, 5 minutes, 4 °C. Tumor samples were incubated with an antibody master mix in FACS buffer (**Table 1**), for 20 minutes 4 °C.

To analyze immune cell frequency in spleens, 5 – 7 spleens were randomly picked per group and approximately a quarter of spleen was mashed through a 40 µm filter into PBS using a syringe plunger. The cell suspension was transferred to FACS tubes and spun down at 390*g*, 5 minutes, 4 °C. Pellet was lysed with 1 ml ACK lysis buffer for 30 seconds while vortexing, to get rid of red blood cells. Samples were diluted by adding 2 ml PBS, spun down and incubated with the antibody master mix in FACS buffer (**Table 2**), for 20 minutes, 4 °C.

After antibody incubation both SQ tumor and spleen samples were washed twice with FACS buffer and fixed in 1% formalin solution (neutral buffered in PBS, Sigma) prior to analysis on a spectral flow cytometer (Sony SP8600).

Table 1. Antibodies used to stain immune cell populations in SQ tumors. All antibodies are purchased from BioLegend and used at 1:333 dilution.

	C2-met SQ tumors		*C2-VTRP1-IV SQ tumors*		*C2-VTPR1-IV4 SQ Tumors*	
Target	**Fluorophore**	**Catalog**	**Fluorophore**	**Catalog**	**Fluorophore**	**Catalog**
CD45	BV711	103147	BV711	103147	BV711	103147
CD11b	FITC	101205	PB	101224	FITC	101205
Ly-6c/Ly-6g (Gr1)	PE-Cy7	108416	PE-Cy7	108416	PE-Cy7	108416
SigF (CD170)	BV421	155509	BV421	155509	BV421	155509
Ly-6c	BV570	128030	BV570	128030	BV570	127629
CD8a	PB	100725	BV785	100750	PB	100725
CD4	APC	100516	BV510	100553	BV510	100553
B220	BV605	103243	BV605	103243	BV605	103243

Table 2. Antibodies used to stain immune cell populations in spleens from mice injected with C2-VTRP1-IV4-SQ1 cells. All antibodies are purchased from BioLegend and used at 1:333 dilution.

Target	Fluorophore	Catalog
CD11b	FITC	101205
Ly-6c/Ly-6g (Gr1)	PE-Cy7	108416
SigF (CD170)	BV421	155509
Ly-6c	BV570	127629
CD8a	PE	100707
B220	PB	103227

Establish primary cell line from mouse metastasis

Macroscopic lung lesions were minced and filtered through 40 µm. Single cells and tumor chunks were cultured in sperate wells of 6-well plate in RPMI complete overnight at 37 °C, 5% CO_2. The next day, cells were carefully washed with PBS to remove dead cells and cultured in RPMI complete until wells reached confluency. Cells were transferred to T25 flasks and treatment with 400 µg/ml geneticin was started. When flasks reached confluency, cells were sorted. For this, cells were resuspended in FACS buffer at a concentration of 1 million/ml and filtered through a 40 µm filter. Only cells with highest zsGreen level were taken (**Figure S2A, S4B**) During sorting, 100,000 – 800,000 cells were collected and cultured in T25 flasks in RPMI complete, supplemented with 400 µg/ml geneticin, 2.5 µg/ml plasmocin (InVivoGen, #ant-mpt) and 250 ng/ml Amphotericin (Gibco, 2328247) for at least 1 week post-sorting.

Protein isolation from cells or tumors

Cells were collected from full T75 plates, spun down, diluted in 1 ml PBS and transferred to Eppendorf tubes. Cells were spun down at 500*g*, 5 minutes, 4 °C and resuspended in lysis buffer (50 mM NaCl (Sigma), 50 mM HEPES (Sigma), 0.5% IGEPAL (Sigma), protease inhibitor (1 tablet in 10 ml, Thermo Fisher) and phosphatase inhibitor (1:100, Sigma) in PBS). Cells are incubated for 30 minutes, 4 °C, shaking (±450 rpm). Debris was spun down at 16,000*g,* 10 minutes, 4 °C. Supernatant was collected, aliquoted and stored at -80 °C.

To isolate proteins from tumors, a small piece of metastasis collected during harvest was flash frozen in liquid nitrogen and stored at -80 °C. Frozen samples were homogenized mechanically with a homogenizer primed with RIPA buffer (1 Pierce Protease Inhibitor tablet (Thermo Fisher) in 10 ml PBS). In between samples, homogenizer was thoroughly washed in HBSS and RIPA buffer. Tissue lysates are spun down at 10,000*g*, 10 minutes, 4 °C. Supernatant was collected, aliquoted and stored at -80 °C.

Western Blot

First, protein concentration of cell or tissue lysate was determined with a Micro BSA Protein assay kit (Thermo Fisher, #23235). OD_{570} was measured at plate reader (PerkinElmer EnVision) and used to calculate protein concentration.

For each sample, 30 µg of protein was collected to which at least 2 µl 6X Lammili SDS-sample buffer (Boston BioProducts) was added. Samples were boiled for 10 minutes at 95 °C, spun down and then loaded on precast gels (MINI PROTEAN TGX, Bio RAD, #4561096 or 4–15% Criterion TGX Precast Midi Protein Gel, Bio RAD #5671094). Precision Plus Protein Dual color standard (Bio RAD, #1610374) ladder was used and empty wells were loaded with SDS-sample buffer. Gel was run in 1x Tris/Glycine/SDS (Boston BioProducts, #BP-150) in demineralized water at 90V.

Proteins were transferred to PVDF membranes (Bio RAD, #1620174 or #1620175) on Trans-Blot Turbo Transfer System (Bio RAD) in transfer stack consisting of Paper Sandwiches (Bio RAD) build according to manufacturer's instructions. Paper sandwiches were submerged in 1x transfer buffer (5x Transfer Buffer (Boston BioProducts, #BP-190), 20% v/v 200 proof ethanol (Decon Laboratories, #3916) in deionized water). Membrane was pretreated with methanol (Sigma) before submerging in 1x transfer buffer. After transfer, membranes were blocked in 5% BSA in TBST (Bovine Serum Albumin, Sigma, #A7906, 20 mM Tris (Sigma), 150 mM NaCl, 0.1% Tween20 (Sigma), pH 7.6) at room temperature (RT), 1 hour, rocking. Membranes were blotted with primary antibodies in 3% BSA in TBST, overnight, 4 °C, rocking. Membranes were washed 3 times, for 10 minutes with TBST and, if necessary, blotted with HRP-conjugated secondary antibodies in 3% BSA in TBST at RT, 1 hour, rocking. MINI or MIDI PVDF membranes were washed 3 times for 10 minutes with TBST and then incubated in 0.5 or 1 mL of Western Lightning Plus-ECL detection reagent (PerkinElmer #NEL103E001EA) respectively, and imaged using a Bio-Rad ChemiDoc Imaging system. Membranes were stripped using Western Blot Stripping buffer (Abcam) for 20 minutes, RT, rocking. The following antibodies were used for western blotting: mouse monoclonal anti-TRP1 (TA99, InVivoMab, #BE0151, diluted 1:5000, **Figure 2F**), rabbit monoclonal anti-TRP1 (PER21960, abcam, #ab235447, 1:1000, **Figure 3G**), rabbit monoclonal anti-beta actin HRP-conjugated (Cell Signaling, #4970S, 1:5000), goat anti-mouse IgG HRP-conjugated (Cell Signalling, #7076S, 1:3333) and goat anti-rabbit IgG HRP-conjugated (Cell Signaling, #7074S, 1:3333).

Priming and cytotoxicity assay

Tumor cells were seeded at 10,000 cells/well in RPMI complete without phenol red (Gibco, #11835-030), supplemented with 0.1 mmol/l B-mercaptoethanol (Sigma, #M6250) and 10 ng/ml recombinant murine interferon gamma (mIFNγ, PeproTech, #315-05) and cultured for ±24 hours at 37 °C, 5% CO_2 in a 96-round bottom well plate.

For C57BL6/J endogenous T-cells or TRP1^{high} T-cells lymphoid organs were harvested as described above. Immune cells were resuspended in 1 ml sterile filtered isolation buffer (2 mM EDTA, 0.1% heat inactivated FBS in PBS). CD8+ T-cells were isolated using EasySep Mouse CD8+ T-cell Isolation Kit (Stem Cell Technologies, #19853) according to manufacturer's instructions. In short, 25 µl of isolation cocktail was added to immune cells at RT, 5 minutes. Rapid spheres were vortexed thoroughly, then 65 µl was added to the cells and incubated at RT, 5 minutes. Cells were further diluted by adding 2 ml isolation buffer, after which conicals were placed in a magnet and supernatant was collected. All cells were counted, spun down and resuspended in RPMI complete without phenol red containing B-mercaptoethanol supplemented with 100 units/ml human IL-2 (PeproTech, #200-02) and 1 µg/ml Ultra-LEAF purified anti-mouse CD28 (BioLegend, #B331922) to a concentration of 500,000 T-cells/ml, unless otherwise stated in figure legend.

T-cells were added to tumor cells in a ratio of 10:1 and incubated for ±72 hours at 37 ^{o}C, 5% CO_2 prior to read-out. As a positive control for activation T-cells were incubated with TRP1 peptide (A1, [32]) at 1 µg/ml instead of tumor cells. For negative control T-cells were seeded without tumor cells.

To assess T-cell activation, cells were spun down, supernatant was discarded using a multichannel and cells were washed in FACS buffer. Antibody master mix (**Table 3**) was added to the wells, and cells were incubated at 4 ^{o}C, 30 minutes. FACS buffer was added, cells were spun and resuspended in 150 µl 1% formalin in PBS. Samples were analyzed on a spectral flow cytometer.

To determine T-cell induced cytotoxicity, isolated T-cells were cultured at 2 million cells/ml in a 6-wells tissue culture plate in 2 ml RPMI complete medium without phenol red supplemented with B-mercaptoethanol and 100 units/ml human IL-2 (PeproTech, #200-02). During the first 48 hours, T-cells were differentiated into effector cells by washed Dynabeads Mouse T-Activator CD3/CD28 for T-Cell Expansion and Activation (1:100. Gibco, #11453D). Effector T-cells were expanded by splitting them 1:2 every 48 hours for 7 – 10 days. For this assay, 10,000 zsGreen tumor cells/well were plated in a 96 well flat bottom black/clear bottom plate (Thermo Fisher, #165305) as described before. After ±24 hours, T-cell number was determined on Celigo Image Cytometer (Nexcelom Bioscience), T-cells were added to tumor cells in a 5:1 ratio, incubated for 48 hours, at 37 ^{o}C, 5% CO_2. Cytotoxicity was determined by comparing zsGreen based confluency of tumor only wells to co-culture wells, measured on image cytometer (Celigo).

Table 3 Antibodies used to stain for T-cell activation. All antibodies are purchased from BioLegend and used at 1:500 dilution.

	C2-VTRP1-IV1, IV2 and IV4 (Figure S3B)		*C2-VTRP1-IV4, IV4-SQ1, IV4-SQ2 (Figure S4D)*	
Target	**Fluorophore**	**Catalog**	**Fluorophore**	**Catalog**
CD45			APC	103112
CD8a	BV785	100750	PB	100725
CD44	BV421	103039	APC-Cy7	103027
CD69	PE	104508	PE	104508
PD-1	APC	562671	PE-Cy7	109109

Immunofluorescence on tumor samples

Mouse SQ tumors or lymph nodes were fixed in aqueous buffer zinc formalin fixative (z-fix, Anatech LTD, #170) for 30 minutes. Fixed samples were incubated in 30% w/v sucrose (Sigma, #59378) in PBS overnight at 4 °C. Half of sucrose was replaced with Optimal Cutting Temperature (OCT, Fisher Healthcare, # 23730571) and samples were further incubated for at least 30 minutes, RT, rocking. Tissues were dried as much as possible, placed in Tissue Trek Cryomolds (Sakura) and imbedded in OCT. Samples were flash frozen on top of liquid nitrogen and stored at -80 °C. Tissue was sectioned on a cryostat (Leica) in 8 µm sections at -22 °C on Frosted Glass Microscope Slides (ASI, #SM2576).

For staining, slides were allowed to thaw to RT for at least 20 minutes, fixed in z-fix for 7 minutes and washed in PBS for 5 minutes before permeabilization in 0.1% Triton-X (PerkinElmer, #N9300260) in PBS three times for 15 minutes, rocking. Tissue on slides was encircled with a hydrophobic pen. Then tissue was blocked in 5% normal goat serum (Abcam, ab7481), 5% glycerol (Sigma) in PBS for 1 hour. Tissue was incubated in primary antibody CD3 – AF594 (Biolegend, #B100240, 1:100 in ±100 µl per tissue) for 1 hour at RT. Slides were washed three times 15 minutes in Triton-X buffer and incubated in DAPI (1:2000) for 15 minutes at RT. Slides were shortly washed in PBS for 5 minutes, air dried and mounted with Prolong Gold antifade (Invitrogen, #P36934) prior to cover slipping. Slides were allowed to harden overnight, before storage at 4 °C.

Microscopy and image processing

Images of live cells in culture were taken on spectral imaging microscope (Olympus IX83 multi-akali PMT) using a 10x objective equipped with the DP74 camera (Olympus) for fluorescence imaging and Hamamatsu camera (Orca Spark) for bright field images. Exposure settings were maintained per channel among samples. Snapshots were taken from representative areas and processed in CellSens Viewer software.

Images of SQ tumors and lymph nodes were taken on a THUNDER wide field microscope (Leica), using a HC PL APO 20x/0.80 objective. Laser power and exposure settings were maintained per channel among samples. Images were processed in Leica LAS X software.

Statistical analysis

Statistical analyses were performed in Prism software (version 9; Graphpad). The tests used to calculate p-values are indicated in figure legends. The number of independent biological or technical repeats per graph is indicated in figure legends.

Results

Depletion of CD4+CD8+ T-cells after tumor resection does not increase the number of macrometastases

In previous experiments utilizing our mouse model of resectable pancreatic cancer, we have shown that our metastatic KPC-C2- SQ-lungmet line (C2-met) is able to metastasize to distant organs such as the lungs and lymph nodes in about 50% of the mice. In combination with the observed low T-cell infiltration in the parental 6694C2 line [16] and the absence of an effect on mouse survival during T-cell depletion in KPC mice [23], we questioned if T-cells can control metastatic outgrowth of the C2-met line in the scope of our novel mouse model.

To test this, we set up an experiment to determine the role of T-cells during the outgrowth of micrometastasis (**Figure 1A**). In short, C2-met cells were subcutaneously injected in the back of wildtype (WT) C57BL/6 mice. After 11 days of growth, the primary tumor was removed and the mice were treated with a cocktail of αCD4/αCD8 antibodies on the day of surgery and two days post-surgery. This antibody treatment depleted all T-cells, including tumor specific T-cells that may have been formed during primary tumor formation allowing us to evaluate T-cell recognition of C2-met cells at metastatic sites.

Interestingly, we find no difference in the metastatic burden of the lungs nor the lymph nodes between the control group and the αCD4/αCD8 treated group (**Figure 1B-D**). As previous experiments in our lab have shown that larger primary tumors tend to metastasize more often (**Figure S1A,** [33]), we confirmed that the weight of primary tumors at resection was similar for both groups (**Figure S1B**). Together, these data show that T-cell depletion does not lead to an increase in metastasis compared to the control group.

We then questioned if the absence of a protective effect of T-cells could be a consequence of a low T-cell response in the primary tumor. We analyzed the primary tumors by flow cytometry and found that the frequency of T-cells in the tumors is indeed very low compared to other immune cell fractions, which is in line with results from the parental C2 cell line [16] (**Figure 1F, Figure S1C, D**). With these results we find that the outgrowth of micrometastasis from C2-met tumors is not controlled by T-cells which may be a consequence of a low T-cell infiltration in the primary tumor or lack of T-cell response.

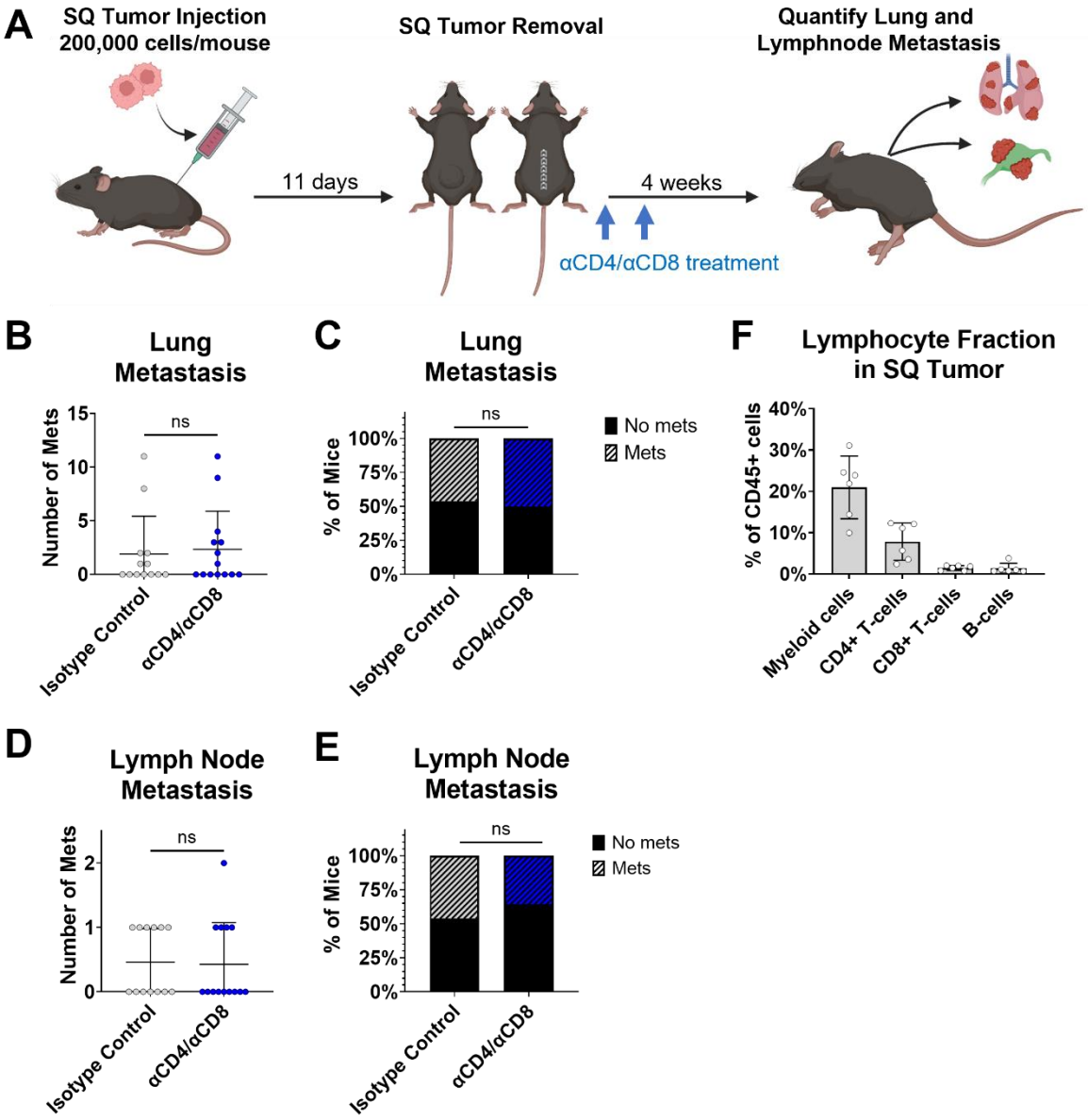

Figure 1. T-cell depletion does not change the number of macrometastasis. (A) Schematic depiction of the experimental set up. Briefly, C57BL6/J mice are subcutaneously (SQ) injected with 200,000 C2-met cells. At 11 days post-injection the tumor is removed and mice are treated with an αCD4 and αCD8 cocktail or isotype control antibodies. Four weeks post-surgery mice are euthanized and metastasis in lung and lymph nodes are counted macroscopically. **(B-E)** Total number of (**B, D**), or percentage of mice with at least 1 (**C, E**), lung (**B,C**) or lymph node (**D, E**) metastasis in isotype control (grey, n=13) or αCD4/αCD8 treated mice (blue, n=14). Data represent mean ± SD of 1 experiment. **(F)** Assessment of lymphocytic immune cell infiltrate in C2-met SQ tumors of isotype treated mice by flow cytometry, shown as the percentage of CD45+ cells. Data represents the mean frequency ± SD (n=5) of 1 experiment. Unpaired t-test was performed to examine the difference in number of lungs and lymph node metastasis between the isotype control (grey) and the αCD4/αCD8 treated mice (blue). Fisher's

exact test was performed to investigate the difference in the percentage of mice with at least 1 lung or lymph node metastasis between isotype and αCD4/αCD8 treated mice. Test results were displayed as not significant (ns) or when significant as *P ≤ 0.05, **P ≤ 0.01, ***P ≤ 0.001 and ****P ≤ 0.0001.

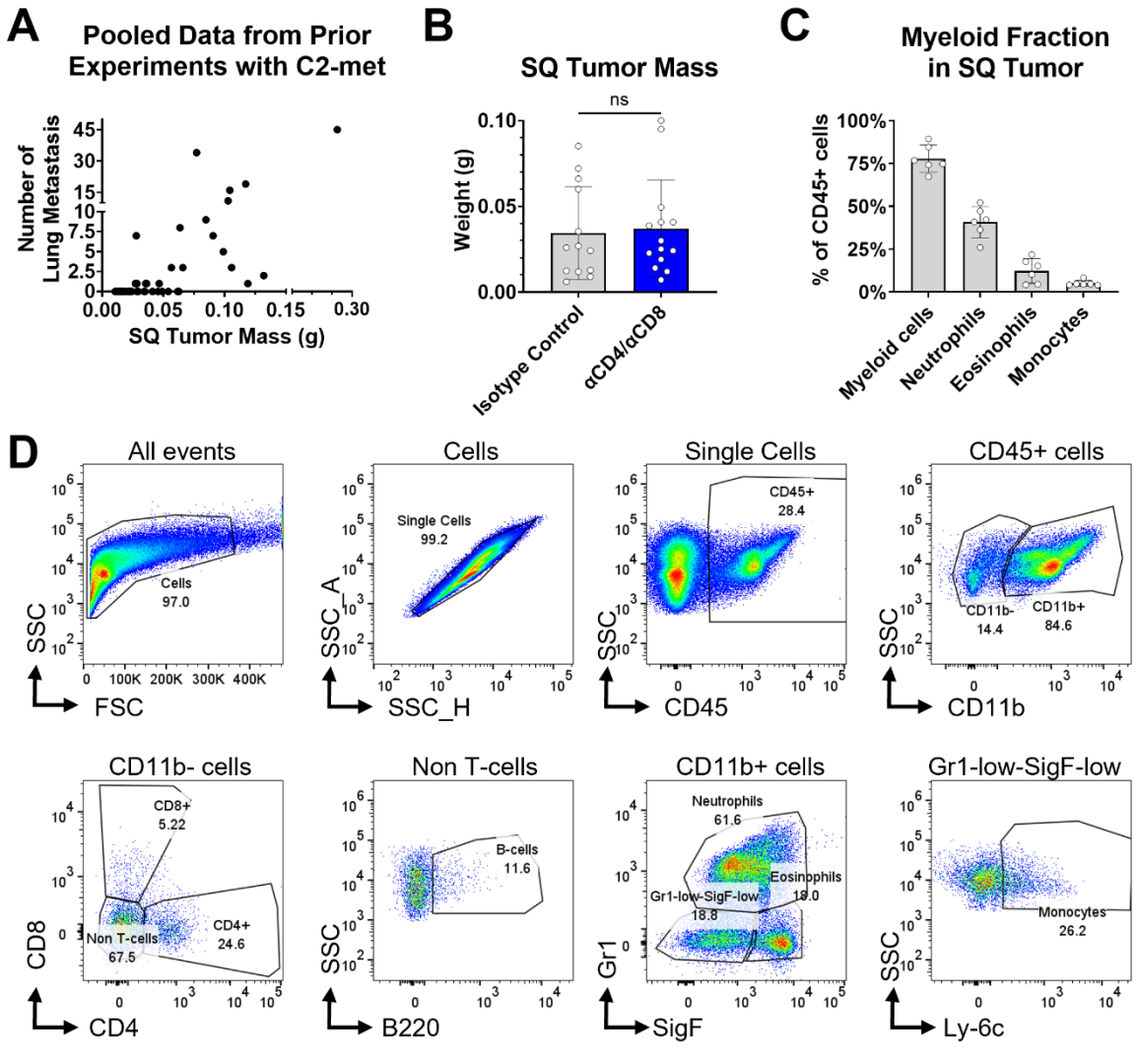

Supplementary Figure 1. C2-met SQ Tumor weight and analysis of SQ immune infiltration. (A) Pooled data from prior experiments with the C2-met line in which tumor weight is plotted against the number of lung metastasis (n=46). **(B)** Weight of resected SQ tumor of isotype control (grey) and αCD4/αCD8 (blue) treated mice. Data represent mean ± SD of 1 experiment. **(C)** Assessment of myeloid immune cell infiltrate in C2-met SQ tumors of isotype treated mice by flow cytometry, shown as the percentage CD45+ cells. Data represents mean frequency ± SD (n=5) of one experiment. **(D)** Flow cytometry gating strategy for immune cells in C2-met SQ tumors. Cells quantified include CD4+ T-cells, CD8+ T-cells, B-cells, eosinophils, neutrophils and monocytes. Unpaired t-test was performed to examine the difference in tumor weight between the isotype control (grey) and the αCD4/αCD8 treated mice (blue).

Test results were displayed as not significant (ns) or when significant as *P ≤ 0.05, **P ≤ 0.01, ***P ≤ 0.001 and ****P ≤ 0.0001.

Derivation and selection of pancreatic cancer cell lines expressing the melanoma self-antigen TRP1

It has been shown that introduction of a strong neoantigen cures mice in a T-cell dependent manner, indicating a role for T-cell control in the presence of a recognizable antigen [23]. To generate a more T-cell responsive C2 cell line, C2 WT cells were transfected with a plasmid expressing both the melanoma self-antigen TRP1 as well as the fluorescent marker zsGreen (**Figure S2A, B**), generating the C2-VTRP1 cell line. The expression of TRP1 on pancreatic cancer cells provides a model to mimic the natural occurrence of tumor antigens with low T-cell receptor affinity and can be used to assess if T-cell recognition alters primary tumor growth or metastatic burden.

Previous experiments in our group have shown that the C2 parental line only metastasizes in 10% of the mice but was increased to over 50% with the C2-met line (**Figure S2C**), which is a line derived from cells that escaped the primary tumor and established in a lung metastasis. We then used a similar approach to derive a metastatic C2-VTRP1 line. We first attempted to develop a metastatic cell line using an intravenous tumor cell injection model to generate lung metastasis [10–12]. C2-VTRP1 cells were injected into the tail vein of 5 mice and lung metastasis were collected 14 days post-injection (**Figure 2A, B**). Several metastases per mouse were processed to isolate metastatic lines which were able to extravasate and colonize the lung (**Figure 2C**). In short, tumors were minced, digested and filtered to retrieve a single cell suspension. Once a cell line was established, the cells were treated with geneticin as the original C2-VTRP1 cells carry a resistance marker on the TRP1/zsGreen plasmid to ensure TRP1 expression (**Figure S2A**). However, even in the presence of geneticin, some cells lost the zsGreen marker (**Figure 2D**). Therefore, we sorted the cells and collected the cell population with the highest mean fluorescence intensity for zsGreen (**Figure S3A**). Western blot analysis found that the sorted cell lines express TRP1, albeit at variable levels (**Figure 2E**). Based on TRP1 expression, we selected cell lines C2-VTRP1-IV1 and IV2 as potential candidates to be used in our mouse model of resectable pancreatic cancer. We also included C2-VTRP1-IV4 as this line grew faster and its mesenchymal morphology (**Figure 2F**) resembled that of the C2-met line (data not shown).

To validate these selected cell lines, we assessed if C2-VTRP1-IV lines can activate naive TRP1^{high} T-cells, which express a high affinity T-cell receptor for TRP1 [31]. For this, T-cells were isolated from a TRP1^{high} mouse and after 72 hours of co-culture, T-cell activation was measured by flow cytometry (**Figure S3B**). We observed clear T-cell activation in the presence of all three IV lines, showing that TRP1 peptides are presented on MHC-I molecules to the T-cells *in vitro*. More importantly, we assessed if TRP1^{high} T-cells can kill the selected cell lines. In order to investigate this, we differentiated TRP1^{high} T-cells into effector cells and co-cultured them with tumor cells. Here, we report that C2-VTrp1-IV4 cells are killed

by TRP1^{high} specific T-cells, while IV1 and IV2, are not (**Figure 2G**). Based on TRP1 expression and the cytotoxicity assay, we selected cell lines C2-VTRP1-IV1, IV2 and IV4 to investigate their metastatic potential in our mouse model of resectable pancreatic cancer.

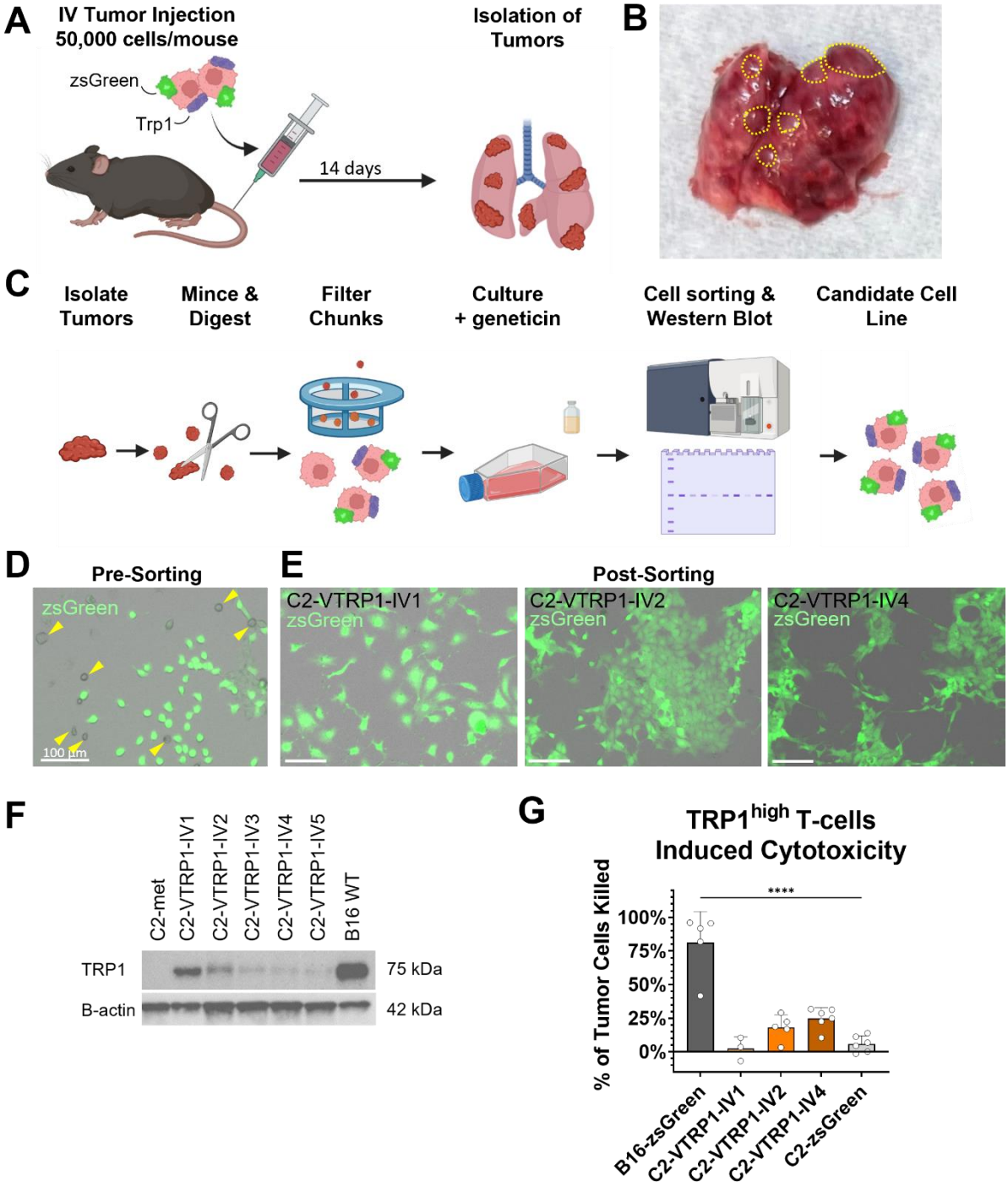

Figure 2. Derivation and validation of metastatic C2-VTRP1 cell lines after intravenous injection. (A) Schematic depiction of experimental set up. Mice were injected with 50,000 C2-VTRP1 cells in the tail vein. Tumors were isolated from the lungs 14 days post-injection. **(B)** Representative photograph showing distinct metastasis (encircled in yellow) in mouse lung. **(C)** Schematic depiction of cell line

generation process. Isolated tumors were minced and digested. The remaining cell suspension was filtered to retrieve single cells. Established lines were grown out in presence of geneticin, then the highest zsGreen expressing cells were selected via sorting. Cell lysates of established sorted populations were taken for Western Blot to verify TRP1 expression. **(D, E)** Representative fluorescence microscopy images showing zsGreen expression (green) in living C2-VTRP1-IV cells pre-sorting (**D**) or post-sorting (**E**). Arrows highlight cells that have lost zsGreen expression pre-sorting. Scale bars: 100 µm. **(F)** Western blot depicting the expression of TRP1 and beta actin of established and sorted C2-VTRP1-IV cell lines, as well as B16 WT (positive control) and C2-met (negative control). **(G)** Assessment of cytotoxicity of B16-zsGreen (dark grey), C2-VTRP1-IV1 (light orange), IV2 (orange), IV4 (dark orange) and C2-zsGreen (light grey) induced by TRP1^{high} T-cells at a ratio of 5:1 tumor cells. Cytotoxicity is depicted as the reduction in zsGreen fluorescence based confluency from tumor only wells to co-culture wells, 48 hours post T-cell addition. Data points represent the mean percentage of killed tumor cells ± SD of at least 3 technical replicates of 1 experiment. One-way ANOVA + Dunnett correction was performed to test for TRP1^{high} T-cell induced cytotoxicity in selected cell lines compared to C2-zsGreen co-culture. Test results were displayed only when significant as *P ≤ 0.05, **P ≤ 0.01, ***P ≤ 0.001 and ****P ≤ 0.0001.

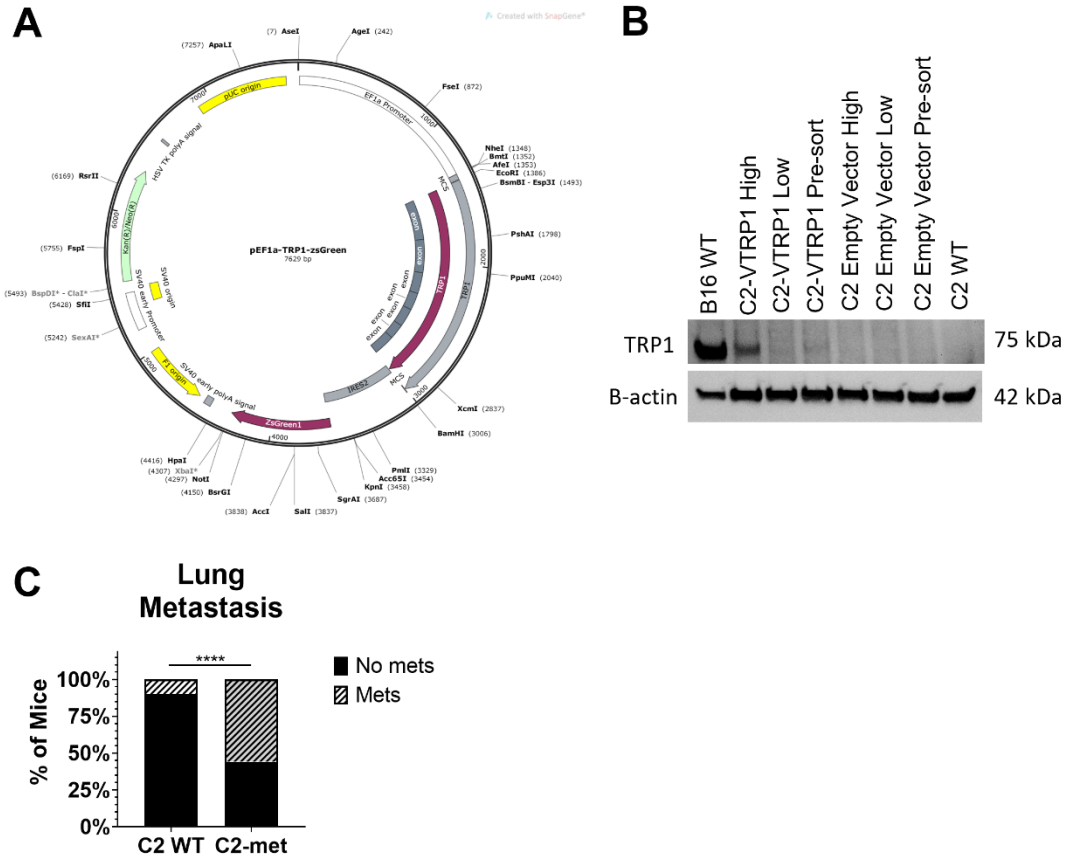

Supplementary Figure 2. TRP1 expression in the non-metastatic C2 WT line (A) Schematic depiction of plasmid containing the *trp1* and *zsgreen* genes behind the pEF1 promotor and resistance genes for kanamycin and neomycin (geneticin) behind a SV40 promotor. **(B)** Western blot depicting the expression of TRP1 and beta actin of sorted C2-VTRP1 cells with either high or low TRP1 level, including B16 (positive control) and C2 lines transfected with empty vectors (negative control). **(C)** Percentage of mice with at least 1 lung metastasis 28 days post resection of SQ tumors grown for 11 days after injection with C2 WT (white, n=30) or C2-met (grey, n=48). Data for C2-met are pooled from 3 independent experiments. Fisher's exact was performed to investigate the difference in percentage of mice with at least 1 lung metastasis after injection with C2 WT or C2-met. Test results were displayed only when significant as *P ≤ 0.05, **P ≤ 0.01, ***P ≤ 0.001 and ****P ≤ 0.0001.

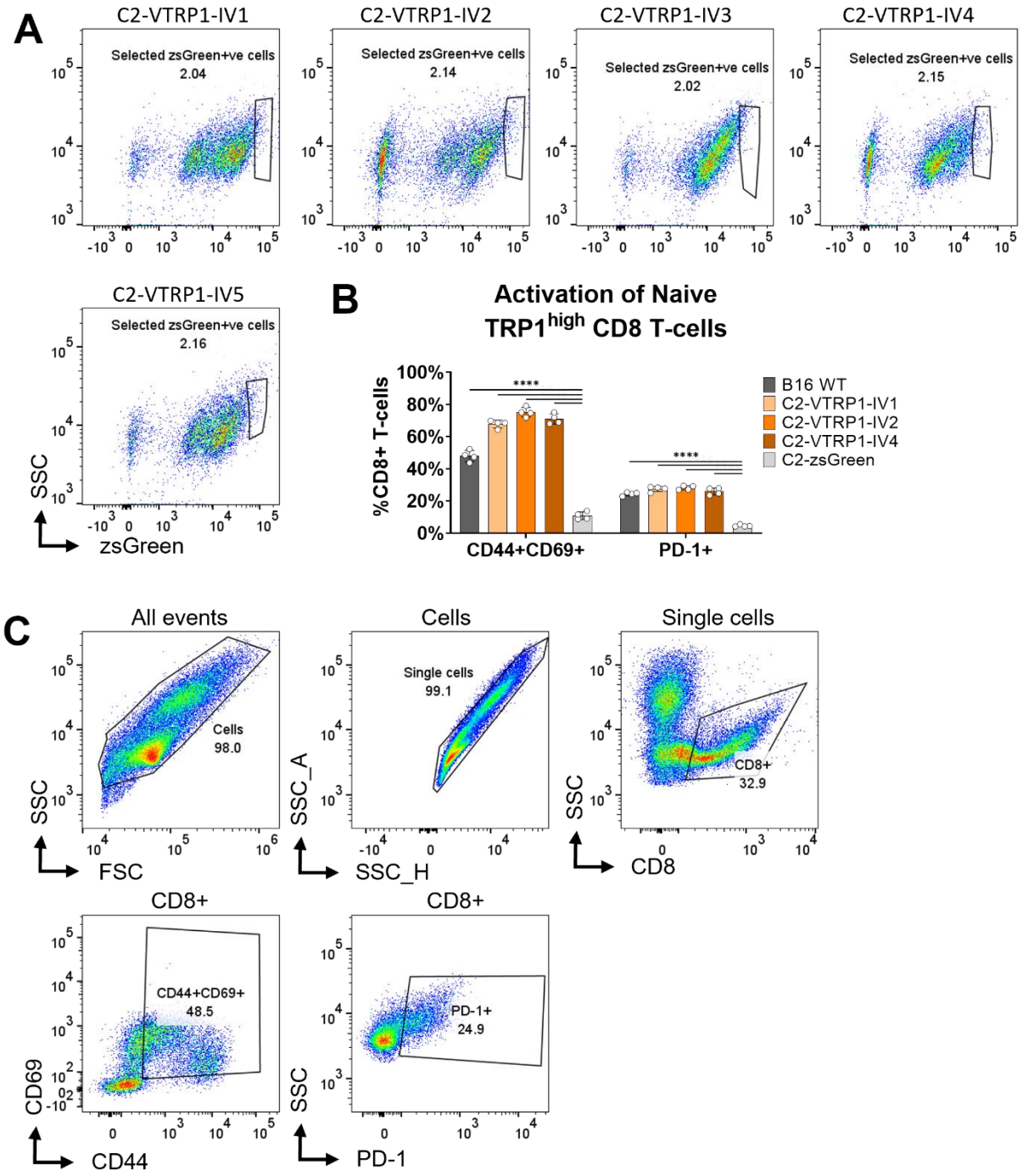

Supplementary Figure 3. Sorted zsGreen+ IV-lines flow cytometry plots and activated TRP1^{high} T-cells. **(A)** Flow cytometry plots illustrating the selected population of zsGreen+ C2-VTRP1-IV populations during sorting. (**B**) Activation of naive TRP1^{high} T-cells by B16 WT (dark grey), C2-VTRP1-IV1 (light orange), IV2 (orange) and IV4 (dark orange) after 72 hours of co-culture in ratio 10:1. C2-zsGreen (light grey) cells were similarly co-cultured with C57BL/6J T-cells as a negative control. Activation is assessed by flow cytometry measuring co-expression of CD44 and CD69 or PD-1. Data represent the mean percentage of positively stained cells ± SD of 4 technical replicates of 1 experiment. (**C**) Flow cytometry gating strategy for T-cell activation markers. Markers quantified include co-expression of CD44 and

CD69, and PD-1. Two-way ANOVA + Dunnett correction was performed to test activation of TRP1^{high} T-cells compared to activation of C57BL/6J T-cells after C2-zsGreen co-culture. Test results were displayed only when significant as *P ≤ 0.05, **P ≤ 0.01, ***P ≤ 0.001 and ****P ≤ 0.0001.

Intravenous injected C2-VTRP1 cells poorly metastasize from the primary tumor

To investigate the metastatic potential of C2-VTrp1-IV1, IV2 and IV4 we injected the cell lines subcutaneously in our mouse model of resectable pancreatic cancer (**Figure 1A**). We resected and weighed the primary tumors 14 days post-injection to standardize tumor sizes to the C2-met line (**Figure 3A**). Flow analysis on the primary tumor revealed a very low T-cell infiltration, irrelevant of the used cell line (**Figure 3B, C, Figure S4A**). These data show that immune cell infiltration is still hampered, despite the presence of the TRP1 antigen in our injected cell lines.

The mice were sacrificed and inspected for macrometastasis 5 weeks post-surgery. Interestingly, only the C2-VTrp1-IV4 line was able to metastasize to the lung (**Figure 3D**). No lymph node metastasis were found in any group. Additionally, the two mice from the C2-VTrp1-IV4 line with lung metastasis only had one metastasis each (**Figure 3E**). Based on these findings, we hypothesized that derivation of metastatic lines from IV tumor cell injection does not provide a sufficient model to generate robustly metastatic C2-VTRP1 cells. IV injection mainly selects for cells that are able to leave the bloodstream and imbed in the lungs, while these cell lines may lack the intrinsic factors that make it possible to escape from the primary tumor and metastasize [15,35].

Since the cells in the lung metastasis have intravasated and extravasated, we again isolated tumor cell lines from the two found metastasis (C2-VTrp1-IV4-SQ1 and SQ2, respectively) (**Figure 2C**). After sorting, we observed that both cell lines grown out from the sorted population (**Figure S4B**) lost zsGreen positivity within a week after sorting, despite co-culturing with geneticin (**Figure 3F, Figure S4C**). To check if the cells also lost TRP1, we assessed TRP1 expression through western blot. Notably, both cell lines expressed TRP1 even at higher levels than the parental C2-VTRP-IV4 line (**Figure 3G**). We also examined if the C2-VTRP1-IV4-SQ lines can activate TRP1^{high} T-cells *in vitro*, to determine if TRP1 peptides are presented on MHC-I molecules. We found that after 72 hours of co-culture C2-VTRP1-IV4-SQ lines are able to significantly increase T-cell activation when compared to C2-zsGreen controls (**Figure S4D,E**). Interestingly, when we investigated if TRP1^{high} T-cells were able to kill C2-VTRP1-IV4-SQ lines, we found no killing (**Figure 3H**). This could suggest that these metastatic cells are resistant to T-cell induced killing *in vitro* [36]. All in all, since the C2-VTRP1-IV4-SQ1 and SQ2 cell lines are both derived from a metastasis, we suggest that they could be a more reliable model to study metastasis in our mouse model of resectable pancreatic cancer in the presence of a recognizable antigen.

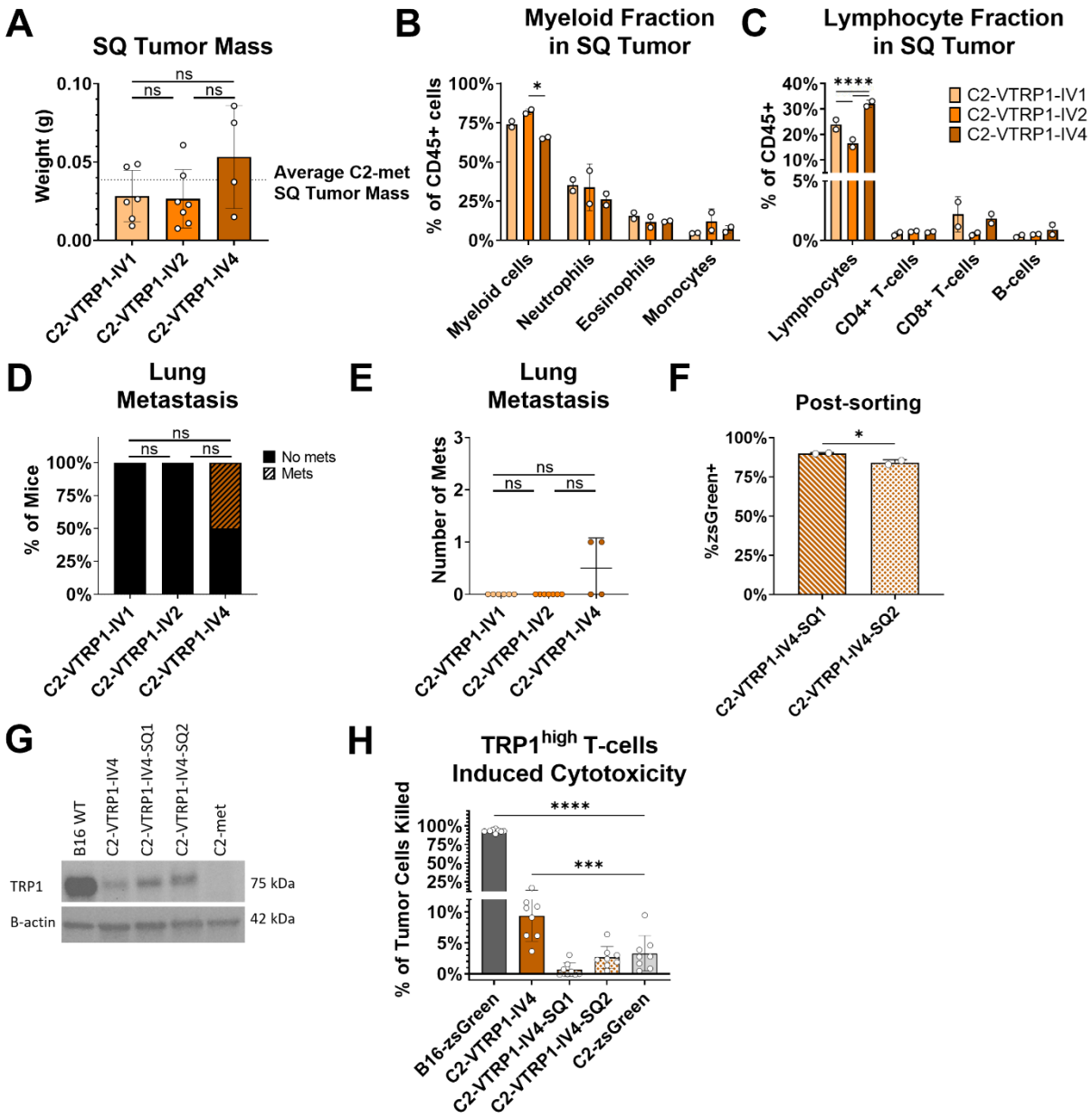

Figure 3. C2-VTRP1-IV lines had low metastatic burden with metastasis selected to generate two new TRP1+ cell lines. (A) Weight of resected C2-VTRP1-IV1 (light orange), IV2 (orange) and IV4 (dark orange) SQ tumor (n=6, 7 and 4 respectively). Data represent mean ± SD of 1 experiment. (**B, C**) Assessment of myeloid (**B**) and lymphocytic (**C**) immune cell infiltrate in C2-VTRP1-IV1, IV2, IV4 SQ tumors by flow cytometry, shown as the percentage of CD45+ cells. Data represents the mean frequency ± SD (n=2) of 1 experiment. **(D, E)** Percentage of mice with at least 1 (**D**) or total number of (**E**) lung metastasis in mice injected with C2-VTRP1-IV1, IV2 or IV4 (n=6, 7 and 4 respectively). Data represent mean ± SD of 1 experiment. **(F)** Percentage of single C2-VTRP1-IV4-SQ1 and SQ2 cells that were zsGreen+ post-sorting. Data represent mean percentage of zsGreen+ cells ± SD of 2 technical replicates of 1 experiment. **(G)** Western blot depicting the expression of TRP1 and beta actin of

established C2-VTRP1-IV4 and SQ cell lines, as well as B16 WT (positive control) and C2-met (negative control). **(H)** Assessment of cytotoxicity of B16-zsGreen (dark grey), C2-VTRP1-IV4 (orange), IV4-SQ1 (dashed orange), IV4-SQ2 (blocked orange) and C2-zsGreen (light gray) induced by $TRP1^{high}$ T-cells at a ratio of 5:1 tumor cells. Cytotoxicity is depicted as the reduction in zsGreen fluorescence based confluency from tumor only wells to co-culture wells, 48 hours post T-cell addition. Data points represent the mean percentage of killed tumor cells ± SD of 8 technical replicates of 1 experiment. One-way ANOVA + Dunnett correction was performed to investigate the difference in SQ tumor weight after injection with C2-VTRP1-IV1, IV2 or IV4. Two-way ANOVA + Dunnets correction was performed to investigate the difference in immune cell infiltration in the SQ tumor, as well as the difference in the number of lung metastasis in mice injected with C2-VTRP1-IV1, IV2 or IV4. Fisher's exact was performed to investigate the difference in percentage of mice with at least 1 lung metastasis after injection with C2-VTRP1-IV1, IV2 or IV4. Unpaired T-test was performed to investigate the difference in zsGreen positivity between C2-VTRP1-IV4-SQ1 and SQ2. One-way ANOVA + Dunnett correction was performed to test for $TRP1^{high}$ T-cell induced cytotoxicity in selected cell lines compared to C2-zsGreen co-culture. Test results were displayed only when significant as *$P \leq 0.05$, **$P \leq 0.01$, ***$P \leq 0.001$ and ****$P \leq 0.0001$, unless all results were not significant (ns).

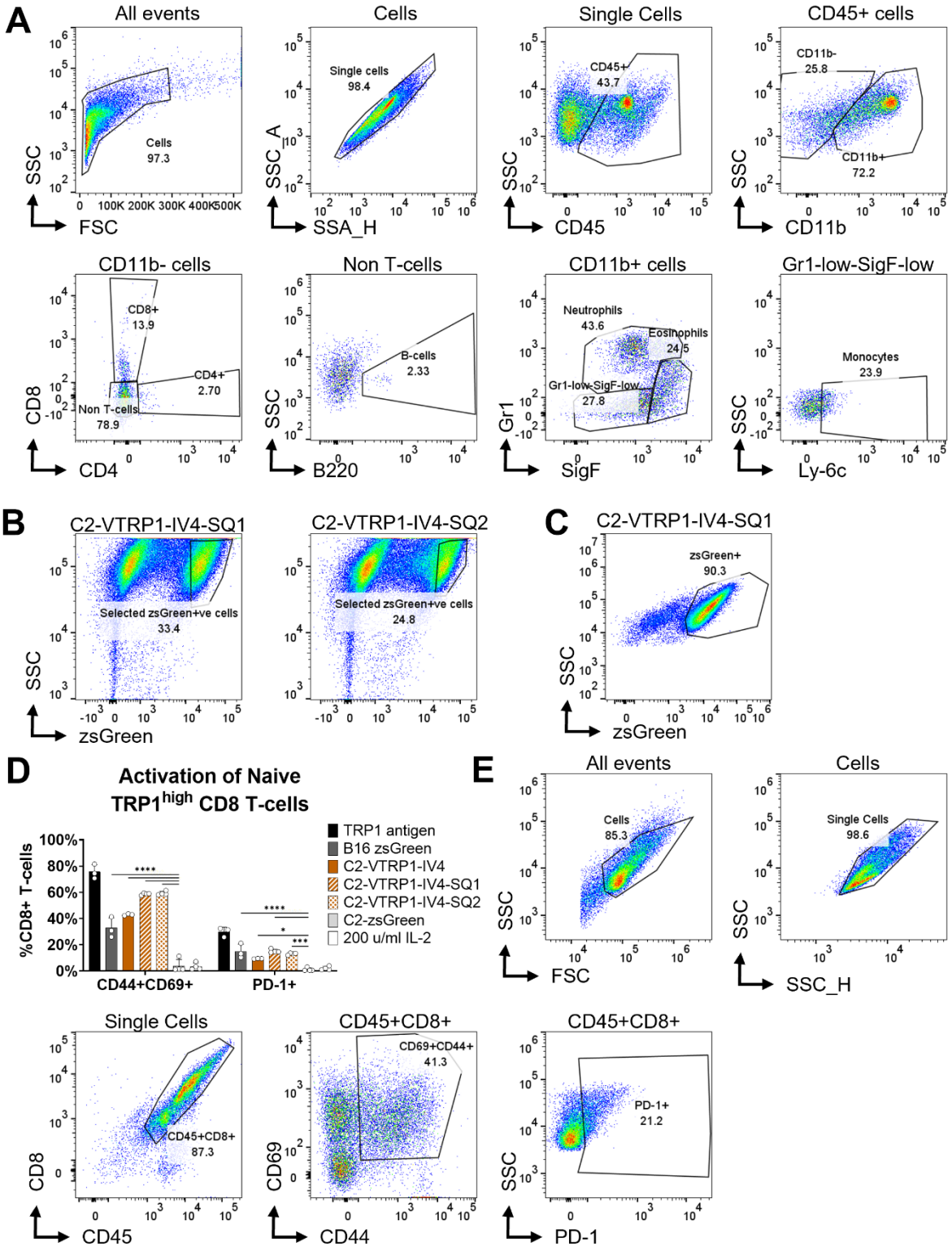

Supplementary Figure 4. Evaluating immune cell presence and activation in the C2-VTRP1-IV4-SQ tumors and lines *in vivo* and *ex vivo*. (A) Flow cytometry gating strategy for immune cells in C2-VTRP1-IV SQ tumors. Cells quantified include CD4+ T cells, CD8+ T-cells, B-cells, eosinophils, neutrophils and monocytes. **(B)** Flow cytometry plots illustrating the sorted zsGreen+ C2-VTRP1-IV4-SQ populations. (**C**) Flow cytometry gating strategy for the percentage of zsGreen+ cells after sorting in C2-VTRP1-IV4-

SQ lines. Displayed plot is from C2-VTRP1-IV4-SQ1 cell line. (**D**) Activation of naive TRP1^{high} T-cells by B16 WT (dark grey), C2-VTRP1-IV4 (dark orange), IV4-SQ1 (dashed orange), IV4-SQ2 (dotted orange) or C2zsGreen (light grey) after 72 hours of co-culture in ratio 10:1. TRP1 A1 peptide (black, 10 ng/ml) served as a positive control and IL-2 only (white, 200 units/ml) served as a negative control. Activation was assessed by flow cytometry measuring co-expression of CD44 and CD69 or PD-1. Data represent the mean percentage of positively stained cells ± SD of 4 technical replicates of 1 experiment. (**E**) Flow cytometry gating strategy for T-cell activation markers. Markers quantified include co-expression of CD44 and CD69, and PD-1. Two-way ANOVA + Dunnett correction was performed to test activation of TRP1^{high} T-cells compared to activation of C57BL/6J T-cells after C2-zsGreen co-culture. Test results were displayed only when significant as *P ≤ 0.05, **P ≤ 0.01, ***P ≤ 0.001 and ****P ≤ 0.0001.

TRP1 expression leads to high CD8 immune infiltration and low metastatic burden

After the establishment of a pancreatic metastatic cell line expressing the melanoma self-antigen TRP1 (C2-VTRP1-IV4-SQ1), we investigated the involvement of the immune system during pancreatic cancer metastasis in our mouse model of resectable pancreatic cancer. First, we evaluated whether TRP1^{high} T-cells can inhibit primary tumor growth and prevent metastasis. In order to study this, we lightly irradiated mice prior to tumor cell injection to aid engraftment of adoptively transferred immune cells isolated from a TRP1^{high} mouse, including TRP1 specific T-cells with high affinity (**Figure 4A**). In addition, repeating our experiment before, we depleted T-cells after surgery in another group of mice with an αCD4/αCD8 cocktail, to investigate if the absence of T-cells increases the number of macrometastasis (**Figure 4A**).

At tumor resection, the tumor mass of the control group was, on average, similar to that of the C2-met tumors (**Figure 4B**), which suggests that any difference in metastatic burden should not be caused by a difference in tumor size. We analyzed immune cell infiltration of the primary tumors to examine the effect of adoptive transfer of TRP1^{high} T-cells. Interestingly, we found an increased lymphocyte infiltration in both isotype control and mice that received TRP1^{high} T-cells, which can be mostly attributed to an enriched CD8+ T-cell population (**Figure 4C, D, Figure S5A**). This indicates that C2-VTRP1-IV4-SQ1 cells may give rise to an immunogenic primary tumor. Remarkedly enough, adoptively transferred TRP1^{high} T-cells did not reduce primary tumor growth, suggesting it may not be a TRP1 uniquely T-cell response.

To investigate the location of the infiltrated T-cells, we performed immunofluorescence (IF). We found staining of T-cells throughout the whole primary C2-VTRP1-IV4-SQ1 tumors (**Figure 4E**). This is in contrast to primary tumors from the C2-met line in which T-cell infiltration is minimal and only observed in the outer edges of the tumor (**Figure 4E**).

Metastatic burden in mouse lungs and lymph nodes was macroscopically assessed 5 weeks post-surgery. Remarkedly, lung and lymph node metastasis are completely absent in the isotype treated mice (**Figure 5A-D**). In the other treatment groups metastasis were found, but the number was much lower compared to the C2-met line, despite similar derivation technique of the metastatic cell line and equal tumor sizes. In line with what we have seen before, depletion of T-cells after resection did not increase the number of observed metastasis. This may suggest that micrometastasis are either not formed or not controlled by T-cells.

We then evaluated the metastases found in treated mice to determine if they potentially downregulated or lost TRP1 expression. We found that TRP1 expression at the metastatic sites is absent or too low to detect (**Figure 5E**). Surprisingly, when we assessed zsGreen expression in the metastatic lymph nodes by immunofluorescence, we observed variable zsGreen fluorescence intensities in each metastasis, regardless of treatment (**Figure 5F**). This could suggest that TRP1 is lost through immunoediting while zsGreen expression is maintained. Additionally, in all metastatic lymph nodes T-cell infiltrations can be found. These infiltrations are distinctly different from those observed in normal lymph nodes, indicating that T-cells are also infiltrating the metastatic sites (**Figure 5G**). This can even be seen in the αCD4/αCD8 treated mice in which CD8+ T-cell population is severely reduced compared to isotype control (**Figure S5B-D**), which suggests that T-cells specifically home to metastatic tumors.

All in all, our study indicates that recognizable tumor antigen expression, in the form of TRP1, in metastatic cell lines reduces their potential to metastasize. Furthermore, our data suggest a distinct role for T-cells in the TRP1 expressing primary tumors which we plan to explore in future work.

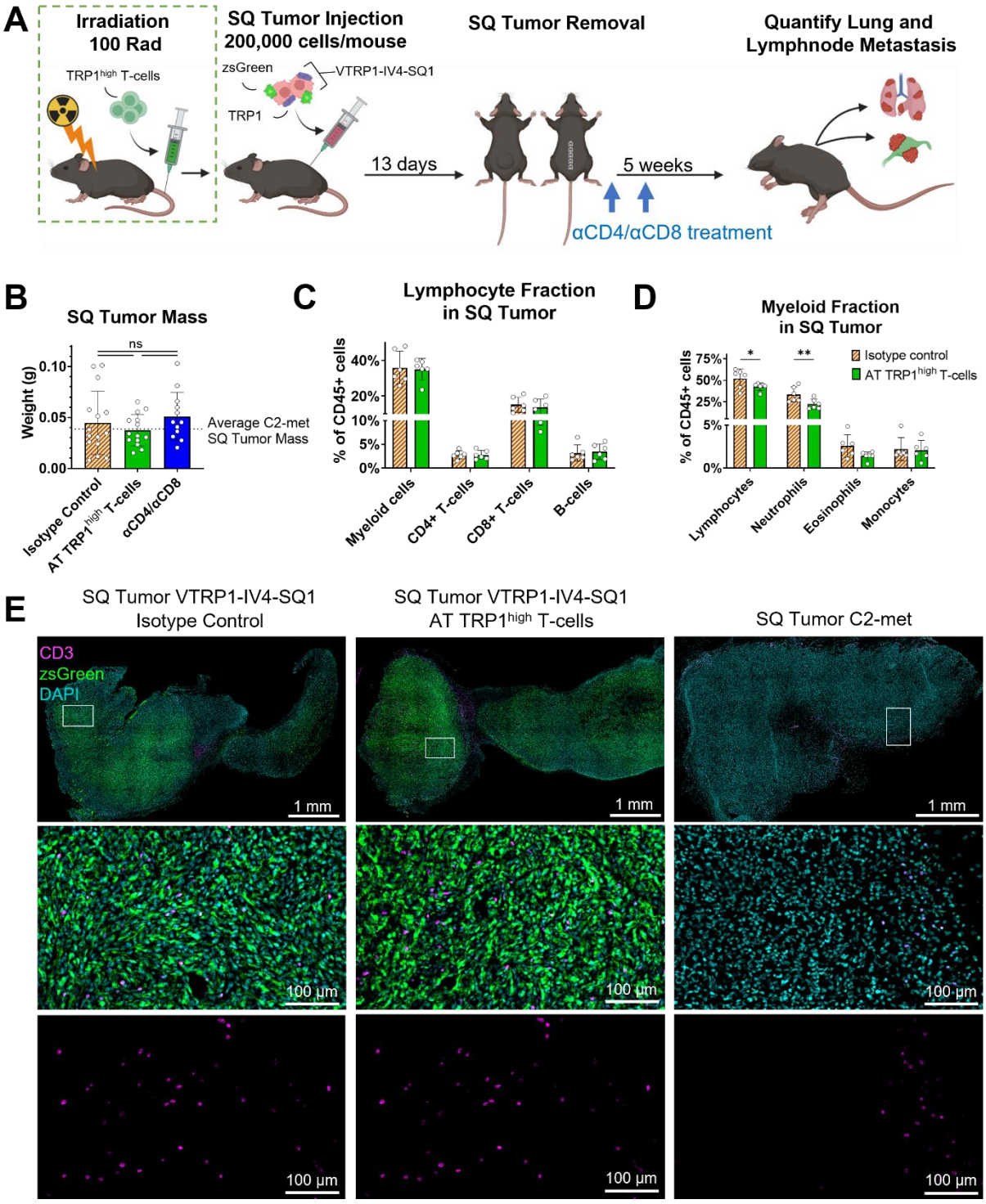

Figure 4. High T-cell infiltration in resected zsGreen expressing C2-VTRP1-SQ1 SQ tumors. (A) Schematic depiction of the experimental set up. Briefly, prior to tumor cell injection mice were sub-lethally irradiated, 4 hours post irradiation immune cells from a TRP1^{high} mouse were adoptively transferred (AT). Following one day for establishment, all mice were subcutaneously (SQ) injected with 200,000 C2-VTRP1-IV4-SQ1 cells which were removed at day 11 along with treatment of an αCD4 and αCD8 cocktail or isotype control antibodies in their respective groups. Metastasis were evaluated four weeks post-surgery. **(B)** Weight of resected C2-VTRP1-IV4-SQ1 SQ tumors of isotype control (dashed

orange, n=15) and αCD4/αCD8 (blue, n=13) treated mice or irradiated + AT TRP1^{high} T-cell mice (green, n=14). Data represent mean ± SD of 1 experiment. (**C, D**) Assessment of lymphocytic (**C**) and myeloid (**D**) immune cell infiltrate by flow cytometry in C2-VTRP1-IV4-SQ1 SQ tumors of isotype control (dashed orange, n=5) treated mice or irradiated mice that received AT TRP1^{high} T-cells (green, n=6), shown as the percentage of CD45+ cells. Data represents the mean frequency ± SD of 1 experiment. **(E)** Representative immunofluorescent (IF) microscopy images of zsGreen expression (green), T-cell infiltration (magenta), with nuclei stained by DAPI (blue) in SQ VTRP1-IV4-SQ1 tumors. Tile scanning image of whole tumor with enlarged subsections. Scale bar = 1 mm and 100 µm, respectively. One-way ANOVA + Tukey correction for multiple comparison was performed to investigate the difference in tumor mass in all different treatment groups. One-way ANOVA + Sidák correction for multiple comparison was performed to investigate differences in immune cell frequencies between isotype control (dashed orange) and irradiated + AT TRP1^{high} T-cell mice (green). Test results were displayed only when significant as *P ≤ 0.05, **P ≤ 0.01, ***P ≤ 0.001 and ****P ≤ 0.0001.

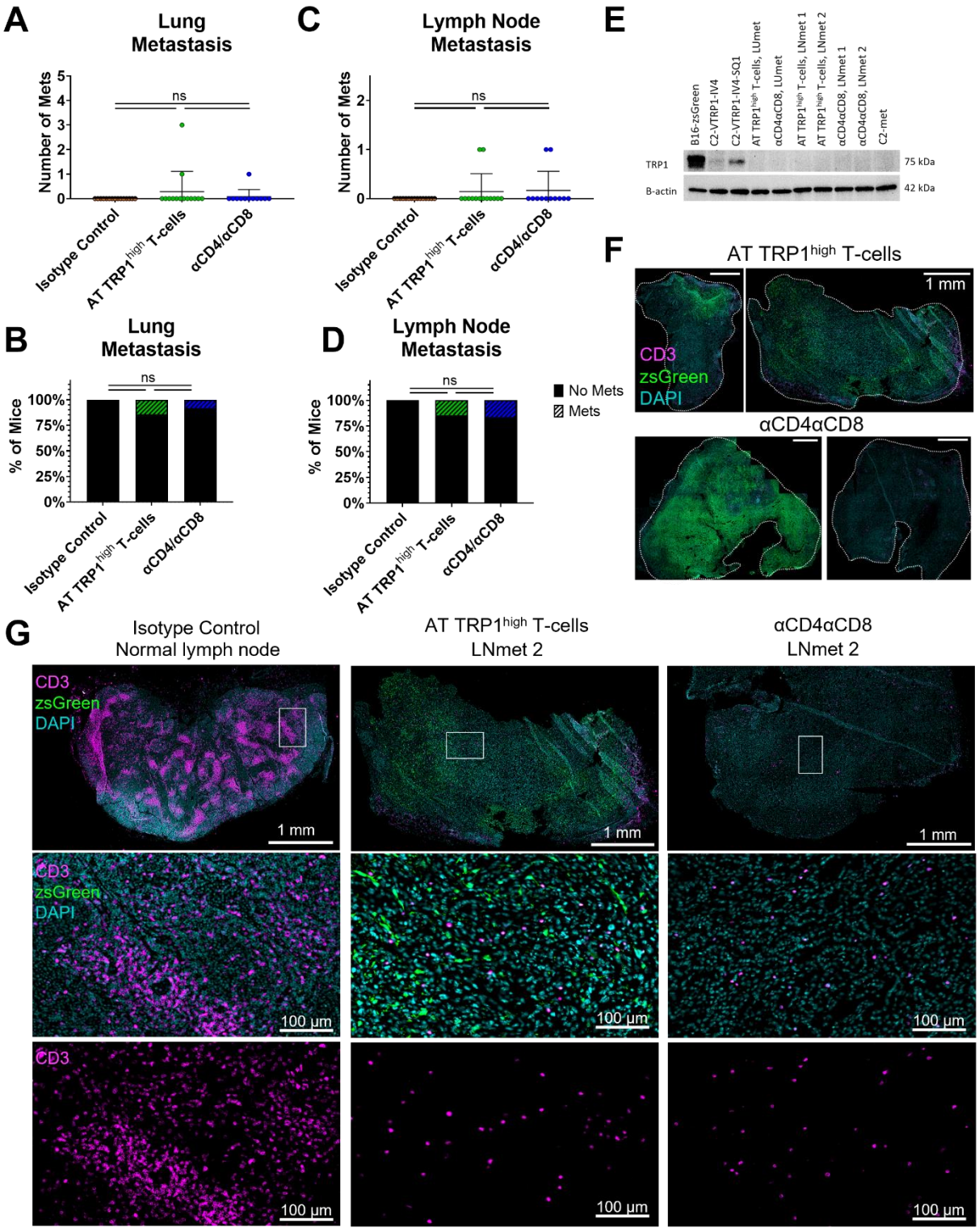

Figure 5. C2-VTRP1-IV4-SQ1 lymph node metastasis are associated with low TRP1 and zsGreen expression. (A-D) Total number of (**A,C**) or percentage of mice with at least 1 (**B,D**) lung (**A**) or lymph node (**C**) metastasis in isotype control (black/orange, n=15), αCD4/αCD8 treated mice (blue, n=13) or irradiated + AT TRP1^{high} T-cell mice (green, n=14). Data represent mean ± SD of 1 experiment. **(E)** Western blot depicting the expression of TRP1 and beta actin of metastatic sites compared to parental lines C2-VTRP1-IV4 and IV4-SQ1. (**F**) Immunofluorescent (IF) microscopy images of zsGreen expression

(green), T-cell infiltration (CD3, magenta), with nuclei stained by DAPI (blue) in all found lymph node metastasis. Tile scanning images of whole lymph node tumors in mice that received AT of TRP1^{high} T-cells (top) or were treated with αCD4αCD8 (bottom). LNmet 1 (left) and LNmet 2 (right) corresponds with lymph node metastases in **E**. Tumors outline is represented by dashed white lines. Scale bar = 1 mm. **(G)** Representative IF microscopy images of zsGreen expression (green), T-cell infiltration (CD3, magenta), with nuclei stained by DAPI (blue) in lymph node metastasis. Tile scanning image of whole lymph node (tumor) with enlarged subsections. Scale bar = 1 mm and 100 µm, respectively. One-way ANOVA + Tukey correction for multiple comparison was performed to investigate the difference in the number of lung or lymph node metastasis between all treatment groups. Fisher's exact test was performed to investigate the difference in the percentage of mice with at least 1 lung and lymph node metastasis between all treatment groups. Test results were displayed as not significant (ns) or when significant as *P ≤ 0.05, **P ≤ 0.01, ***P ≤ 0.001 and ****P ≤ 0.0001.

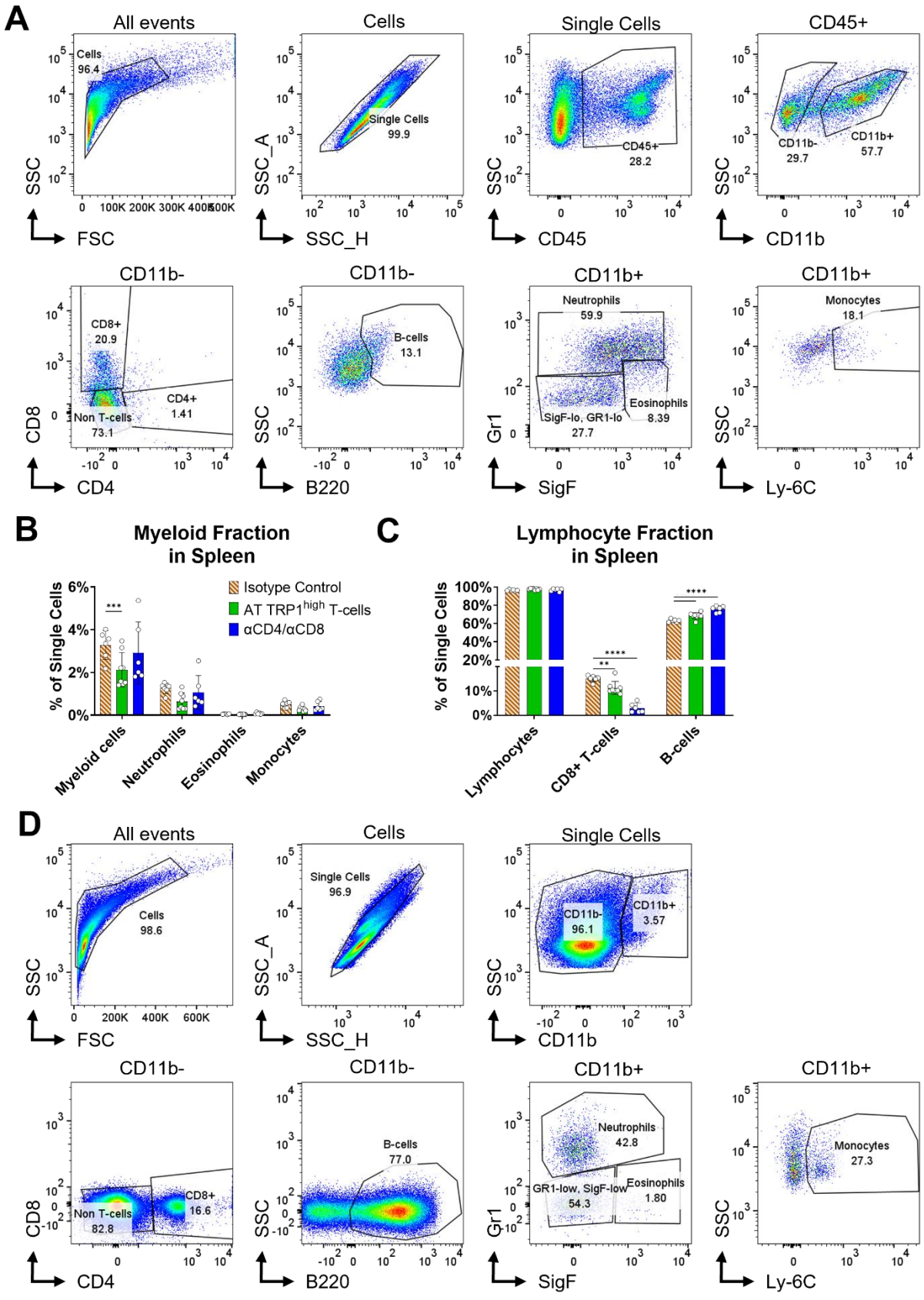

Supplementary Figure 5. Flow cytometry analysis of immune cells from C2-VTRP1-IV4-SQ1 SQ tumors and spleens. (A) Flow cytometry gating strategy for immune cells in C2-VTRP1-IV4-SQ1 SQ

tumors. Cells quantified include CD4+ T-cells, CD8+ T-cells, B-cells, eosinophils, neutrophils and monocytes,. (**B&C**) Assessment of myeloid (**B**) and lymphocytic (**C**) immune cell infiltrate by flow cytometry in spleens of isotype control (dashed orange, n=6), αCD4/αCD8 treated mice and (blue, n=6) and irradiated + AT TRP1^{high} T-cell mice (green, n=8), shown as the percentage of all single cells. Data represents the mean frequency ± SD of 1 experiment. **(D)** Flow cytometry gating strategy for immune cells in spleens. Cells quantified include CD8+ T-cells, B-cells, eosinophils, neutrophils and monocytes. One-way ANOVA + Dunnett correction for multiple comparisons was performed to investigate the difference in immune cell frequencies between isotype control (dashed orange), αCD4/αCD8 treated mice and (blue) and mice that received AT of TRP1^{high} T-cells (green). Test results were displayed only when significant as *P ≤ 0.05, **P ≤ 0.01, ***P ≤ 0.001 and ****P ≤ 0.0001.

Discussion

The aim of this study was to investigate T-cell associated immunity during PDAC metastasis in the presence of a recognizable tumor antigen. We have found that expression of TRP1 in C2-VTRP1-IV4-SQ1 tumors greatly increases CD8+ T-cell infiltration in the primary tumor. In multiple studies, CD8+ T-cell infiltration has been associated with tumor control and a reduced metastatic burden [37,38]. In line with this, the metastatic rate of C2-VTRP1-IV4-SQ1 is very low. To clarify if TRP1 recognition by T-cells is responsible for the reduced occurrence of metastasis, we aim to deplete CD4+/CD8+ T-cells during primary tumor formation or inject our C2-VTRP1-IV4-SQ1 cells in RAG2-/- mice, lacking T- and B-cells [39]. The absence of T-cell control, will also shed light on the metastatic potential of our cell lines. Alternatively, if we find that the TRP1 expressing cells still metastasize poorly, we could transfect C2-met cells with TRP1 and inject those in (T-cell deficient) mice. This would clarify if TRP1 expression reduced metastasis in a T-cell dependent manner or if C2-VTRP1-IV4-SQ1 cells lack intrinsic factors that are necessary for a metastatic cell line [40,41].

Metastatic behavior is not only linked to intrinsic factors, such as the expression of neoantigens or genes associated with metastatic cells [42,43], but also related to tumor extrinsic factors. Notably, we found that C2-VTRP1-IV4 tumors have a very low CD8+ T-cell infiltration compared to C2-VTRP1-IV4-SQ1 tumors. This is especially interesting since we have found that C2-VTRP1-IV4-SQ1 and SQ2 are not killed by TRP1^{high} T-cells *in vitro*, despite TRP1 expression. This raises the question whether TRP1 expression is solely responsible for the increased CD8+ T-cell or that there are other tumor extrinsic factors at play. In previous studies, it has been shown that adoptive transfer of TRP1 specific T-cells completely eradicated B16 tumors but only in RAG2 -/- mice, not in WT mice [44], indicating an inhibitory effect from other T- or B-cells. Research in pancreatic cancer has stressed that that regulatory T-cells (Tregs) can suppress T-cell priming and CD8+ T-cell activity [16,45–47]. Investigation

690 of Treg presence in C2-VTRP1-IV4-SQ1 tumors, C2-VTRP1-IV4 tumors or even C2-met tumors, would
691 shed light on possible differences in tumor suppression.
692 Uninhibited growth of the primary tumor while preventing metastasis, has been observed in several
693 studies [48–50] and is referred to as concomitant immunity [51]. This phenomenon raises the
694 hypothesis that the TRP1 expressing primary tumor could function as a form of vaccination to the
695 immune system. However, in our study the presence of adoptively transferred $TRP1^{high}$ T-cells was not
696 enough to diminish tumor growth, which might indicate that TRP1 specific tumor cells alone are not
697 sufficient to prevent tumor growth or even metastasis. We hypothesize that TRP1 expression aids the
698 initial immune response, which then results in a broader immune response against multiple epitopes
699 [52,53]. In mice implanted with KPC-OVA cells this epitope spreading has been observed, and when
700 rechallenged with WT KPC cells, resulted in tumor resistance or rejection [23]. Through adoptive
701 transfer of the immune system of C2-VTRP1-IV4-SQ1 tumor-bearing mice to naive mice prior to
702 injection with C2-VTRP1-IV4-SQ1 or C2-met cells, we can evaluate if these tumors are immunologically
703 controlled by T-cells not only specific for TRP1 [48].
704 The opposite of epitope spreading, which is induction of immune tolerance, has also been shown using
705 PDAC cells expressing the OVA antigen. Mice in which RMA OVA cells were subcutaneously implanted,
706 exhibited a profound immune response [54]. Such a response was completely absent in mice that were
707 first intravenously exposed to LB27 OVA expressing cells and then challenged by subcutaneous
708 injection of RMA OVA cells [54]. These data introduced the idea of CD8+ T-cell tolerance induction
709 through uptake of tumor antigens from circulating apoptotic tumor cells into the liver or spleen
710 [55,56]. These tumor antigens can also be presented to CD4+ T-cells promoting differentiation into
711 Tregs [57]. Based on these findings we hypothesize that C2-met tumors could induce immune
712 tolerance to C2-VTRP1-IV4-SQ1 tumors due to recognition of antigens on circulating tumor cells. Our
713 mouse model of resectable pancreatic cancer provides us with a platform in which we can effectively
714 study immune tolerance in mice that are (re)challenged after tumor resection or intravenously injected
715 with killed C2-met cells [58].
716 Lastly, the presence of tumor specific immune cells can lose its value when tumor cells become less
717 immunogenic. It has been shown in both mice and humans, that lymphocyte killing of immunogenic
718 cancer cells often causes less immunogenic clones to dominate the population [59–61]. In our study,
719 we have seen that lymph node metastasis which have seeded from C2-VTRP1-IV4-SQ1 tumors have
720 reduced TRP1 and zsGreen expression when compared to the primary tumors. This indicates that
721 throughout the metastatic process, cancer cells have downregulated or even lost TRP1/zsGreen. To
722 examine if this is due to immunoediting it would be valuable to investigate TRP1 presence at metastatic
723 sites in RAG2 -/- mice.

All in all, we found that expression of the melanoma self-antigen TRP1 in C2 pancreatic cancers cells, reverses their T-cell low phenotype to a T-cell high phenotype and is associated with reduced metastatic burden. Further research needs to elucidate whether this is the cause of TRP1 expression alone or if there are other tumor intrinsic factors at play. Metastasis that did occur, have undetectable TRP1 expression and reduced zsGreen expression, which indicates that TRP1 presence induces immunoediting. In conclusion, a metastatic pancreatic cancer cell line expressing a recognizable self-antigen provides many new possibilities to study the involvement of the immune system in pancreatic cancer metastasis.

Reference list

1. Werner, J.; Combs, S.E.; Springfeld, C.; Hartwig, W.; Hackert, T.; Büchler, M.W. Advanced-Stage Pancreatic Cancer: Therapy Options. *Nature Reviews Clinical Oncology 2013 10:6* **2013**, *10*, 323–333, doi:10.1038/nrclinonc.2013.66.

2. Saad, A.M.; Turk, T.; Al-Husseini, M.J.; Abdel-Rahman, O. Trends in Pancreatic Adenocarcinoma Incidence and Mortality in the United States in the Last Four Decades; a SEER-Based Study. *BMC Cancer* **2018**, *18*, doi:10.1186/S12885-018-4610-4.

3. Oba, A.; Ho, F.; Bao, Q.R.; Al-Musawi, M.H.; Schulick, R.D.; Chiaro, M. del Neoadjuvant Treatment in Pancreatic Cancer. *Front Oncol* **2020**, *10*, 245, doi:10.3389/FONC.2020.00245.

4. American Cancer Society Survival Rates for Pancreatic Cancer Available online: https://www.cancer.org/cancer/pancreatic-cancer/detection-diagnosis-staging/survival-rates.html (accessed on 11 August 2022).

5. He, C.; Huang, X.; Zhang, Y.; Cai, Z.; Lin, X.; Li, S. A Quantitative Clinicopathological Signature for Predicting Recurrence Risk of Pancreatic Ductal Adenocarcinoma After Radical Resection. *Front Oncol* **2019**, *9*, 1197, doi:10.3389/FONC.2019.01197/BIBTEX.

6. Pongprasobchai, S.; Pannala, R.; Smyrk, T.C.; Bamlet, W.; Pitchumoni, S.; Ougolkov, A.; de Andrade, M.; Petersen, G.M.; Chari, S.T. Long-Term Survival and Prognostic Indicators in Small (≤2 Cm) Pancreatic Cancer. *Pancreatology* **2008**, *8*, 587, doi:10.1159/000161009.

7. He, C.; Cai, Z.; Zhang, Y.; Lin, X. Comparative Recurrence Analysis of Pancreatic Adenocarcinoma after Resection. *J Oncol* **2021**, *2021*, doi:10.1155/2021/3809095.

8. Hingorani, S.R.; Wang, L.; Multani, A.S.; Combs, C.; Deramaudt, T.B.; Hruban, R.H.; Rustgi, A.K.; Chang, S.; Tuveson, D.A. Trp53R172H and KrasG12D Cooperate to Promote Chromosomal Instability and Widely Metastatic Pancreatic Ductal Adenocarcinoma in Mice. *Cancer Cell* **2005**, *7*, 469–483, doi:10.1016/j.ccr.2005.04.023.

9. Lee, J.W.; Komar, C.A.; Bengsch, F.; Graham, K.; Beatty, G.L. Genetically Engineered Mouse Models of Pancreatic Cancer: The KPC Model (LSL-KrasG12D/+;LSL-Trp53R172H/+;Pdx-1-Cre), Its Variants and Their Application in Immuno-Oncology Drug Discovery. *Current protocols in pharmacology / editorial board, S.J. Enna (editor-in-chief) ... [et al.]* **2016**, *73*, 14.39.1, doi:10.1002/CPPH.2.

10. Franses, J.W.; Philipp, J.; Missios, P.; Bhan, I.; Liu, A.; Yashaswini, C.; Tai, E.; Zhu, H.; Ligorio, M.; Nicholson, B.; et al. Pancreatic Circulating Tumor Cell Profiling Identifies LIN28B as a Metastasis Driver and Drug Target. *Nature Communications 2020 11:1* **2020**, *11*, 1–12, doi:10.1038/s41467-020-17150-3.

11. Roe, J.S.; Hwang, C. il; Somerville, T.D.D.; Milazzo, J.P.; Lee, E.J.; da Silva, B.; Maiorino, L.; Tiriac, H.; Young, C.M.; Miyabayashi, K.; et al. Enhancer Reprogramming Promotes Pancreatic Cancer Metastasis. *Cell* **2017**, *170*, 875, doi:10.1016/J.CELL.2017.07.007.

12. Matsuda, Y.; Yoshimura, H.; Ueda, J.; Naito, Z.; Korc, M.; Ishiwata, T. Nestin Delineates Pancreatic Cancer Stem Cells in Metastatic Foci of NOD/Shi-Scid IL2Rγnull (NOG) Mice. *Am J Pathol* **2014**, *184*, 674, doi:10.1016/J.AJPATH.2013.11.014.

13. Kong, K.; Guo, M.; Liu, Y.; Zheng, J. Progress in Animal Models of Pancreatic Ductal Adenocarcinoma. *J Cancer* **2020**, *11*, 1555, doi:10.7150/JCA.37529.

14. Miquel, M.; Zhang, S.; Pilarsky, C. Pre-Clinical Models of Metastasis in Pancreatic Cancer. *Front Cell Dev Biol* **2021**, *9*, doi:10.3389/FCELL.2021.748631.

15. Gomez-Cuadrado, L.; Tracey, N.; Ma, R.; Qian, B.; Brunton, V.G. Mouse Models of Metastasis: Progress and Prospects. *Dis Model Mech* **2017**, *10*, 1061, doi:10.1242/DMM.030403.

16. Li, J.; Byrne, K.T.; Yan, F.; Yamazoe, T.; Chen, Z.; Baslan, T.; Richman, L.P.; Lin, J.H.; Sun, Y.H.; Rech, A.J.; et al. Tumor Cell-Intrinsic Factors Underlie Heterogeneity of Immune Cell Infiltration and Response to Immunotherapy. *Immunity* **2018**, *49*, 178, doi:10.1016/J.IMMUNI.2018.06.006.

17. Stromnes, I.M.; Hulbert, A.; Pierce, R.H.; Greenberg, P.D.; Hingorani, S.R. T-Cell Localization, Activation, and Clonal Expansion in Human Pancreatic Ductal Adenocarcinoma. *Cancer Immunol Res* **2017**, *5*, 978, doi:10.1158/2326-6066.CIR-16-0322.

18. de Santiago, I.; Yau, C.; Heij, L.; Middleton, M.R.; Markowetz, F.; Grabsch, H.I.; Dustin, M.L.; Sivakumar, S. Immunophenotypes of Pancreatic Ductal Adenocarcinoma: Meta-analysis of Transcriptional Subtypes. *Int J Cancer* **2019**, *145*, 1125, doi:10.1002/IJC.32186.

19. Timmer, F.E.F.; Geboers, B.; Nieuwenhuizen, S.; Dijkstra, M.; Schouten, E.A.C.; Puijk, R.S.; de Vries, J.J.J.; Petrousjka van den Tol, M.; Bruynzeel, A.M.E.; Streppel, M.M.; et al. Pancreatic Cancer and Immunotherapy: A Clinical Overview. *Cancers (Basel)* **2021**, *13*, doi:10.3390/CANCERS13164138.

20. Karamitopoulou, E. The Tumor Microenvironment of Pancreatic Cancer. *Cancers (Basel)* **2020**, *12*, 1–4, doi:10.3390/CANCERS12103076.

21. Waddell, N.; Pajic, M.; Patch, A.M.; Chang, D.K.; Kassahn, K.S.; Bailey, P.; Johns, A.L.; Miller, D.; Nones, K.; Quek, K.; et al. Whole Genomes Redefine the Mutational Landscape of Pancreatic Cancer. *Nature 2015 518:7540* **2015**, *518*, 495–501, doi:10.1038/nature14169.

22. Alexandrov, L.B.; Nik-Zainal, S.; Wedge, D.C.; Aparicio, S.A.J.R.; Behjati, S.; Biankin, A. v.; Bignell, G.R.; Bolli, N.; Borg, A.; Børresen-Dale, A.L.; et al. Signatures of Mutational Processes in Human Cancer. *Nature 2013 500:7463* **2013**, *500*, 415–421, doi:10.1038/nature12477.

23. Evans, R.A.; Diamond, M.S.; Rech, A.J.; Chao, T.; Richardson, M.W.; Lin, J.H.; Bajor, D.L.; Byrne, K.T.; Stanger, B.Z.; Riley, J.L.; et al. Lack of Immunoediting in Murine Pancreatic Cancer Reversed with Neoantigen. *JCI Insight* **2016**, *1*, 88328, doi:10.1172/JCI.INSIGHT.88328.

24. Rooryck, C.; Roudaut, C.; Robine, E.; Müsebeck, J.; Arveiler, B. Oculocutaneous Albinism with TYRP1 Gene Mutations in a Caucasian Patient. *Pigment Cell Res* **2006**, *19*, 239–242, doi:10.1111/J.1600-0749.2006.00298.X.

25. Curran, M.A.; Montalvo, W.; Yagita, H.; Allison, J.P. PD-1 and CTLA-4 Combination Blockade Expands Infiltrating T Cells and Reduces Regulatory T and Myeloid Cells within B16 Melanoma Tumors. *Proc Natl Acad Sci U S A* **2010**, *107*, 4275, doi:10.1073/PNAS.0915174107.

26. Leick, K.M.; Pinczewski, J.; Mauldin, I.S.; Young, S.J.; Deacon, D.H.; Woods, A.N.; Bosenberg, M.W.; Engelhard, V.H.; Slingluff, C.L. Patterns of Immune Cell Infiltration in Murine Models of Melanoma: Roles of Antigen and Tissue Site in Creating Inflamed Tumors. *Cancer Immunol Immunother* **2019**, *68*, 1121, doi:10.1007/S00262-019-02345-5.

27. Bertolotto, C.; Bille, K.; Ortonne, J.-P.; Bauotti, R. Regulation of Tyrosinase Gene Expression by CAMP in B16 Melanoma Cells Involves Two CATGTG Motifs Surrounding the TATA Box: Implication of the Microphthalmia Gene Product. *J Cell Biol* **1996**, *134*, 747–755.

28. Ralli, M.; Botticelli, A.; Visconti, I.C.; Angeletti, D.; Fiore, M.; Marchetti, P.; Lambiase, A.; de Vincentiis, M.; Greco, A. Immunotherapy in the Treatment of Metastatic Melanoma: Current Knowledge and Future Directions. *J Immunol Res* **2020**, *2020*, doi:10.1155/2020/9235638.

29. Aleksic, M.; Liddy, N.; Molloy, P.E.; Pumphrey, N.; Vuidepot, A.; Chang, K.M.; Jakobsen, B.K. Different Affinity Windows for Virus and Cancer-Specific T-Cell Receptors – Implications for Therapeutic Strategies. *Eur J Immunol* **2012**, *42*, 3174, doi:10.1002/EJI.201242606.

30. Chinnasamy, D.; Tran, E.; Yu, Z.; Morgan, R.A.; Restifo, N.P.; Rosenberg, S.A. Simultaneous Targeting of Tumor Antigens and the Tumor Vasculature Using T Lymphocyte Transfer Synergize to Induce Regression of Established Tumors in Mice. *Cancer Res* **2013**, *73*, 3371, doi:10.1158/0008-5472.CAN-12-3913.

31. Dougan, S.K.; Dougan, M.; Kim, J.; Turner, J.A.; Ogata, S.; Cho, H. il; Jaenisch, R.; Celis, E.; Ploegh, H.L. Transnuclear TRP1-Specific CD8 T Cells with High or Low Affinity TCRs Show Equivalent Anti-Tumor Activity. *Cancer Immunol Res* **2013**, *1*, 99, doi:10.1158/2326-6066.CIR-13-0047.

32. Clancy-Thompson, E.; Devlin, C.A.; Tyler, P.M.; Servos, M.M.; Ali, L.R.; Ventre, K.S.; Aladdin Bhuiyan, M.; Bruck, P.T.; Birnbaum, M.E.; Dougan, S.K. Altered Binding of Tumor Antigenic Peptides to MHC Class I Affects T Cell-Effector Responses. *Cancer Immunol Res* **2018**, *6*, 1524, doi:10.1158/2326-6066.CIR-18-0348.

33. Ansari, D.; Bauden, M.; Bergström, S.; Rylance, R.; Marko-Varga, G.; Andersson, R. Relationship between Tumour Size and Outcome in Pancreatic Ductal Adenocarcinoma. *British Journal of Surgery* **2017**, *104*, 600–607, doi:10.1002/BJS.10471.

34. Blando, J.; Sharma, A.; Higa, M.G.; Zhao, H.; Vence, L.; Yadav, S.S.; Kim, J.; Sepulveda, A.M.; Sharp, M.; Maitra, A.; et al. Comparison of Immune Infiltrates in Melanoma and Pancreatic Cancer Highlights VISTA as a Potential Target in Pancreatic Cancer. *Proc Natl Acad Sci U S A* **2019**, *116*, 1692–1697, doi:10.1073/PNAS.1811067116/SUPPL_FILE/PNAS.1811067116.SAPP.PDF.

35. Seyfried, T.N.; Huysentruyt, L.C. On the Origin of Cancer Metastasis. *Crit Rev Oncog* **2013**, *18*, 43, doi:10.1615/CRITREVONCOG.V18.I1-2.40.

36. Lemoine, J.; Ruella, M.; Houot, R. Born to Survive: How Cancer Cells Resist CAR T Cell Therapy. *J Hematol Oncol* **2021**, *14*, 1–12, doi:10.1186/S13045-021-01209-9/TABLES/2.

37. Peske, J.D.; Woods, A.B.; Engelhard, V.H. Control of CD8 T-Cell Infiltration into Tumors by Vasculature and Microenvironment. *Adv Cancer Res* **2015**, *128*, 263, doi:10.1016/BS.ACR.2015.05.001.

38. Li, K.; Li, T.; Feng, Z.; Huang, M.; Wei, L.; Yan, Z.; Long, M.; Hu, Q.; Wang, J.; Liu, S.; et al. CD8+ T Cell Immunity Blocks the Metastasis of Carcinogen-Exposed Breast Cancer. *Sci Adv* **2021**, *7*, 8936–8954, doi:10.1126/SCIADV.ABD8936/SUPPL_FILE/SCIADV.ABD8936_SM.PDF.

39. Milsom, C.C.; Lee, C.R.; Hackl, C.; Man, S.; Kerbel, R.S. Differential Post-Surgical Metastasis and Survival in SCID, NOD-SCID and NOD-SCID-IL-2Rγnull Mice with Parental and Subline Variants of Human Breast Cancer: Implications for Host Defense Mechanisms Regulating Metastasis. *PLoS One* **2013**, *8*, doi:10.1371/JOURNAL.PONE.0071270.

40. Celià-Terrassa, T.; Kang, Y. Distinctive Properties of Metastasis-Initiating Cells. *Genes Dev* **2016**, *30*, 892, doi:10.1101/GAD.277681.116.

41. Leone, K.; Poggiana, C.; Zamarchi, R. The Interplay between Circulating Tumor Cells and the Immune System: From Immune Escape to Cancer Immunotherapy. *Diagnostics* **2018**, *8*, 59, doi:10.3390/DIAGNOSTICS8030059.

42. Bournet, B.; Pointreau, A.; Souque, A.; Oumouhou, N.; Muscari, F.; Lepage, B.; Senesse, P.; Barthet, M.; Lesavre, N.; Hammel, P.; et al. Gene Expression Signature of Advanced Pancreatic Ductal Adenocarcinoma Using Low Density Array on Endoscopic Ultrasound-Guided Fine Needle Aspiration Samples. *Pancreatology* **2012**, *12*, 27–34, doi:10.1016/J.PAN.2011.12.003.

43. Carstens, J.L.; Yang, S.; Correa de Sampaio, P.; Zheng, X.; Barua, S.; McAndrews, K.M.; Rao, A.; Burks, J.K.; Rhim, A.D.; Kalluri, R. Stabilized Epithelial Phenotype of Cancer Cells in Primary Tumors Leads to Increased Colonization of Liver Metastasis in Pancreatic Cancer. *Cell Rep* **2021**, *35*, 108990, doi:10.1016/J.CELREP.2021.108990.

44. Xie, Y.; Akpinarli, A.; Maris, C.; Hipkiss, E.L.; Lane, M.; Kwon, E.K.M.; Muranski, P.; Restifo, N.P.; Antony, P.A. Naive Tumor-Specific CD4+ T Cells Differentiated in Vivo Eradicate Established Melanoma. *J Exp Med* **2010**, *207*, 651, doi:10.1084/JEM.20091921.

45. Zhang, Y.; Lazarus, J.; Steele, N.G.; Yan, W.; Lee, H.J.; Nwosu, Z.C.; Halbrook, C.J.; Menjivar, R.E.; Kemp, S.B.; Sirihorachai, V.R.; et al. Regulatory T Cell Depletion Alters the Tumor Microenvironment and Accelerates Pancreatic Carcinogenesis. *Cancer Discov* **2020**, *10*, 422, doi:10.1158/2159-8290.CD-19-0958.

46. Siret, C.; Collignon, A.; Silvy, F.; Robert, S.; Cheyrol, T.; André, P.; Rigot, V.; Iovanna, J.; van de Pavert, S.; Lombardo, D.; et al. Deciphering the Crosstalk Between Myeloid-Derived Suppressor Cells and Regulatory T Cells in Pancreatic Ductal Adenocarcinoma. *Front Immunol* **2020**, *10*, 3070, doi:10.3389/FIMMU.2019.03070/BIBTEX.

47. Ware, M.B.; El-Rayes, B.F.; Lesinski, G.B. Mirage or Long-Awaited Oasis: Reinvigorating T-Cell Responses in Pancreatic Cancer. *J Immunother Cancer* **2020**, *8*, e001100, doi:10.1136/JITC-2020-001100.

48. Alicke, B.; Totpal, K.; Schartner, J.M.; Berkley, A.M.; Lehar, S.M.; Capietto, A.H.; Cubas, R.A.; Gould, S.E. Immunization Associated with Primary Tumor Growth Leads to Rejection of

Commonly Used Syngeneic Tumors upon Tumor Rechallenge. *J Immunother Cancer* **2020**, *8*, 532, doi:10.1136/JITC-2020-000532.

49. Joosten, J.J.A.; v. Muijen, G.N.P.; Wobbes, T.; Ruers, T.J.M. In Vivo Destruction of Tumor Tissue by Cryoablation Can Induce Inhibition of Secondary Tumor Growth: An Experimental Study. *Cryobiology* **2001**, *42*, 49–58, doi:10.1006/cryo.2001.2302.

50. Gorelik, E. Concomitant Tumor Immunity and the Resistance to a Second Tumor Challenge. *Adv Cancer Res* **1983**, *39*, 71–120, doi:10.1016/S0065-230X(08)61033-7.

51. Janssen, L.M.E.; Ramsay, E.E.; Logsdon, C.D.; Overwijk, W.W. The Immune System in Cancer Metastasis: Friend or Foe? *Journal for ImmunoTherapy of Cancer 2017 5:1* **2017**, *5*, 1–14, doi:10.1186/S40425-017-0283-9.

52. Lo, J.A.; Kawakubo, M.; Juneja, V.R.; Su, M.Y.; Erlich, T.H.; LaFleur, M.W.; Kemeny, L. v.; Rashid, M.; Malehmir, M.; Alireza Rabi, S.; et al. Epitope Spreading toward Wild-Type Melanocyte-Lineage Antigens Rescues Suboptimal Immune Checkpoint Blockade Responses. *Sci Transl Med* **2021**, *13*, doi:10.1126/SCITRANSLMED.ABD8636/SUPPL_FILE/ABD8636_SM.PDF.

53. Das, M.; Zhou, X.; Liu, Y.; Das, A.; Vincent, B.G.; Li, J.; Liu, R.; Huang, L. Tumor Neoantigen Heterogeneity Impacts Bystander Immune Inhibition of Pancreatic Cancer Growth. *Transl Oncol* **2020**, *13*, doi:10.1016/J.TRANON.2020.100856.

54. Berg, M.; Wingender, G.; Djandji, D.; Hegenbarth, S.; Momburg, F.; Hämmerling, G.; Limmer, A.; Knolle, P. Cross-Presentation of Antigens from Apoptotic Tumor Cells by Liver Sinusoidal Endothelial Cells Leads to Tumor-Specific CD8+ T Cell Tolerance. *Eur J Immunol* **2006**, *36*, 2960–2970, doi:10.1002/EJI.200636033.

55. Ugel, S.; Peranzoni, E.; Desantis, G.; Chioda, M.; Walter, S.; Weinschenk, T.; Ochando, J.C.; Cabrelle, A.; Mandruzzato, S.; Bronte, V. Immune Tolerance to Tumor Antigens Occurs in a Specialized Environment of the Spleen. *Cell Rep* **2012**, *2*, 628–639, doi:10.1016/J.CELREP.2012.08.006.

56. Li, B.; Zhang, S.; Huang, N.; Chen, H.; Wang, P.; Li, J.; Pu, Y.; Yang, J.; Li, Z. Dynamics of the Spleen and Its Significance in a Murine H22 Orthotopic Hepatoma Model. *Exp Biol Med* **2016**, *241*, 863, doi:10.1177/1535370216638772.

57. Wei, S.; Kryczek, I.; Zou, W. Regulatory T-Cell Compartmentalization and Trafficking. *Blood* **2006**, *108*, 426, doi:10.1182/BLOOD-2006-01-0177.

58. Green, D.R.; Ferguson, T.; Zitvogel, L.; Kroemer, G. IMMUNOGENIC AND TOLEROGENIC CELL DEATH. *Nat Rev Immunol* **2009**, *9*, 353, doi:10.1038/NRI2545.

59. Matsushita, H.; Vesely, M.D.; Koboldt, D.C.; Rickert, C.G.; Uppaluri, R.; Magrini, V.J.; Arthur, C.D.; White, J.M.; Chen, Y.S.; Shea, L.K.; et al. Cancer Exome Analysis Reveals a T-Cell-Dependent Mechanism of Cancer Immunoediting. *Nature 2011 482:7385* **2012**, *482*, 400–404, doi:10.1038/nature10755.

60. Shankaran, V.; Ikeda, H.; Bruce, A.T.; White, J.M.; Swanson, P.E.; Old, L.J.; Schreiber, R.D. IFNγ and Lymphocytes Prevent Primary Tumour Development and Shape Tumour Immunogenicity. *Nature 2001 410:6832* **2001**, *410*, 1107–1111, doi:10.1038/35074122.

61. Łuksza, M.; Sethna, Z.M.; Rojas, L.A.; Lihm, J.; Bravi, B.; Elhanati, Y.; Soares, K.; Amisaki, M.; Dobrin, A.; Hoyos, D.; et al. Neoantigen Quality Predicts Immunoediting in Survivors of Pancreatic Cancer. *Nature 2022 606:7913* **2022**, *606*, 389–395, doi:10.1038/s41586-022-04735-9.